CHAPTER 9
FUSION PRODUCT DIAGNOSTICS

M. SASAO* *Tohoku University, Sendai 980-8579, Japan*

T. NISHITANI *Japan Atomic Energy Agency, Naka, Ibaraki 319-0195, Japan*

A. KRASILNILOV *SRC RF TRINITI, Troitsk, Russia*

S. POPOVICHEV and V. KIPTILY *EURATOM—UKAEA Fusion Association Culham S.C., OX14 3DB, United Kingdom*

J. KALLNE *Uppsala University, Department of Neutron Research, Uppsala, Sweden*

Received January 22, 2007
Accepted for Publication September 10, 2007

Fusion product diagnostics can be used to determine a fusion reaction rate, which indicates how close the plasma is to the ultimate goal of making a power plant based on nuclear fusion. However, these diagnostics can also provide large amounts of additional information, such as ion temperatures, the thermonuclear fraction in the fusion reaction rate, degree of fast ion confinement, fast ion loss mechanism, etc. Measurement systems for fusion product diagnostics are usually designed and optimized to a specific performance so that they play different roles in the experiment. The neutron emission rate, which is directly related to the fusion output, can be determined by (a) time-resolved emission monitors, which are well calibrated on-site, in combination with (b) activation systems and (c) profile monitors with accuracy up to several percent. The time-resolved neutron profiles also provide useful information for transport analysis. Velocity distributions and confinement properties of fast ions can be obtained from (d) the neutron spectrometers and (e) gamma-ray measurement. The interaction between plasma dynamics and fast ions can be studied with most fusion product diagnostic systems, especially with (f) escaping charged fusion product detectors. Each section of this chapter contains a general explanation of these systems, showing some experimental results obtained on present devices. A lot of interesting and useful information on the behavior of energetic particles and their degree of confinement are provided by them because interaction between thermal and nonthermal energetic ions and that among nonthermal ions contribute dominantly to the fusion reaction rate in present deuterium-deuterium experiments. In future deuterium-tritium fusion experiments on ITER, the contribution of thermonuclear fraction will be increased, and the combination of several neutron measurement systems will provide the absolute fusion output and neutron fluence on the first wall. Together with neutron measurement, alpha particle and gamma-ray measurement play important roles in research on self-heating burning plasma physics and hence in the burning control of the device.

KEYWORDS: *neutron measurement, alpha-particle measurement, gamma-ray measurement*

Note: Some figures in this paper are in color only in the electronic version.

Contents—Chapter 9

*E-mail: mamiko.sasao@qse.tohoku.ac.jp

I. INTRODUCTION

Fusion product diagnostics can be categorized into two groups based on the information that can be obtained: the neutron production rate from a plasma and the amount and behaviors of energetic ions. The former indicates how closely the plasma in a fusion device under a specific operation scenario approaches the ultimate goal of a self-sustained nuclear fusion reactor. A representative of the former group is measurement of neutron emission rate, while a representative of the latter group is escaping/loss alpha-particle measurement. The confinement of energetic ions, which can be studied from the latter group, is of primary importance for fusion reactor development because the 3.5-MeV alpha particles produced through deuterium-tritium (D-T) fusion reactions

$$\mathrm{D} + \mathrm{T} \rightarrow {}^4\mathrm{He}\ (3.5\ \mathrm{MeV}) + n\ (14.1\ \mathrm{MeV})\ , \qquad (1)$$

act as an energy source to heat the plasma, thus resulting in a self-sustaining reaction. This is referred to as a burning plasma or an ignited plasma, and devices aimed at obtaining self-sustaining fusion plasmas are known as burning plasma devices. The confinement of alpha particles is one of the key issues of ITER, which is now under construction with international collaboration as a burning plasma device.

Although definite conclusions from intensive research on ITER are anticipated, a great deal of information can be obtained from current fusion devices with deuterium plasmas. Here, deuterium-deuterium (D-D) reactions

$$d + d \rightarrow t\ (1.0\ \mathrm{MeV}) + p\ (3.0\ \mathrm{MeV}) \qquad (2)$$

and

$$d + d \rightarrow {}^3\mathrm{He}\ (0.82\ \mathrm{MeV}) + n\ (2.45\ \mathrm{MeV}) \qquad (3)$$

have been the primary diagnostic tools, and the D-^{3}He reaction

$$d + {}^3\mathrm{He} \rightarrow {}^4\mathrm{He}\ (3.7\ \mathrm{MeV}) + p\ (14.7\ \mathrm{MeV}) \qquad (4)$$

has been used for diagnosing the plasma when ^{3}He gas is introduced for the discharge.

Cross sections for these reactions can simply be calculated by tunneling probability through a potential barrier,[1] which is composed by a repulsive long-range Coulomb potential and an attractive short-range nuclear potential. This probability is known to have an energy dependency of $\exp(-1/E^{1/2})$. It has an additional energy dependency of $1/E$, which comes from a cross section of $\pi\lambda^2$ (λ: the de Broglie wavelength). This can be expressed as

$$\sigma(E) = \frac{a}{E}\exp\left(-\frac{b}{E^{1/2}}\right)\ , \qquad (5)$$

where a and b are parameters to be calculated. The shape and height of the potential barrier include complicated physics, such as Coulomb screening.[2] On the other hand, cross sections have been measured experimentally with considerable accuracy down to the 10 keV region,[3] and parameters can be obtained by the fitting procedure. Better parametrization of the cross section[4] has been done as a function of the ion energy in various forms, such as

$$\sigma(E) = \frac{S(E)}{E}\exp\left(-\frac{b}{E^{1/2}}\right)$$

and

$$S(E) = \frac{A_1 + E(A_2 + E(A_3 + E(A_4 + EA_5)))}{1 + E(B_1 + E(B_2 + E(B_3 + EB_4)))}\ . \qquad (6)$$

Here, A_1, A_2, A_3, A_4, A_5, B_1, B_2, B_3, B_4, and b are parameters obtained by adjustment to both the theoretical calculation and the experimental data,[4] and the curves shown in Fig. 1a were calculated using these parameters. The strong energy dependence of the fusion cross section can be seen, but that of the D-T reaction has a peak in the relatively low-energy region ~100 keV. This is one of the main reasons why first-generation fusion reactors use the D-T reaction.

The reactivity is defined as the product of the cross section and the relative velocity averaged over the velocity distribution in a Maxwellian plasma and can be parameterized as a function of the ion temperature in expressions such as

$$\langle\sigma v\rangle = C_1\theta\sqrt{\frac{\xi}{m_r c^2 T^3}}\,e^{-3\xi}\ , \qquad (7)$$

where

$$\theta = T\Big/\left[1 - \frac{T(C_2 + T(C_4 + TC_6))}{1 + T(C_3 + T(C_5 + TC_7))}\right]$$

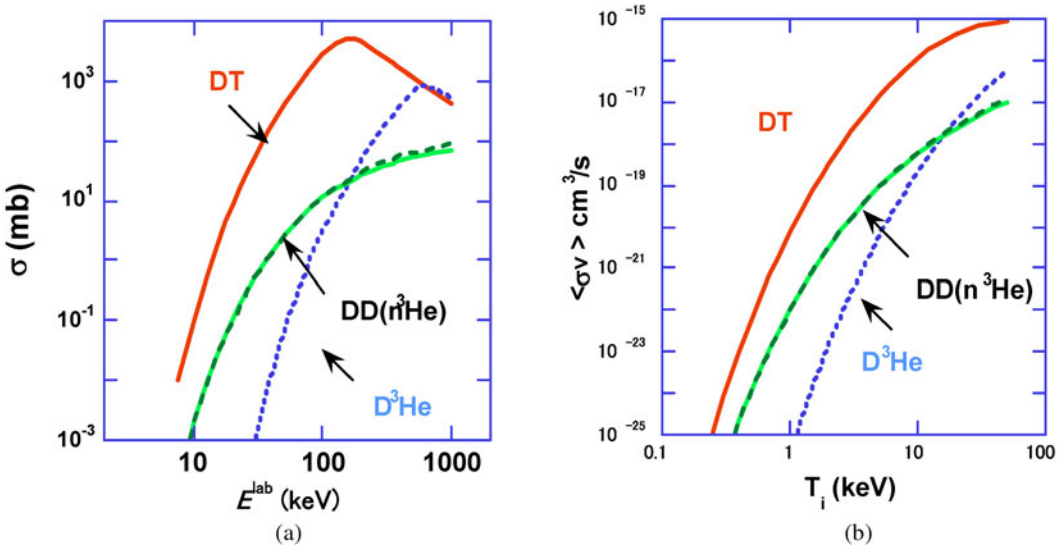

Fig. 1. Fusion cross sections as a function of the CM energy of the reacting particles (a) and fusion reactivities for Maxwellian ion distributions as a function of ion temperature T_i (b).

and

$$\xi = \left(\frac{B_G^2}{4\pi}\right)^{1/3} \quad , \quad B_G = \pi\alpha Z_1 Z_2 \sqrt{2 m_r c^2} \quad ,$$

where B_G is called the Gamov constant[5] and $m_r c^2$ is the reduced mass of the particles. Parameters C_1, C_2, C_3, C_4, C_5, C_6, C_7 are tabulated in Ref. 4, and the curves shown in Fig. 1b were calculated using these parameters.

In most cases, a plasma contains nonthermal energetic ions originating from neutral beam injection (NBI) or accelerated by waves of ion cyclotron range frequency (ICRF), and the ion velocity distribution can be separated into thermal and beam components. Then, the actual reaction rate in a plasma of a unit volume, $Y_{total}(t)$, is comprised of three terms: a thermonuclear term, $Y_{th}(t)$; a beam thermal term, $Y_{b\text{-}th}(t)$; and a beam-beam term, $Y_{b\text{-}b}(t)$:

$$Y_{total} = Y_{th} + Y_{b\text{-}th} + Y_{b\text{-}b} \tag{8}$$

and

$$\begin{cases} Y_{th} = n_j n_i \langle \sigma v \rangle_{Ti} & j \neq i \\ Y_{th} = \frac{1}{2} n_i^2 \langle \sigma v \rangle_{Ti} & j = i \end{cases} \tag{9}$$

where

$$Y_{b\text{-}th} = n_b n_i \langle \sigma v \rangle_{b\text{-}th} \quad , \quad Y_{b\text{-}b} = \tfrac{1}{2} n_b^2 \langle \sigma v \rangle_{b\text{-}b} \quad , \tag{10}$$

and

$$\langle \sigma v \rangle_{12} = \iint f_1(\vec{v}_1) f_2(\vec{v}_2) \sigma(v_{rel}) v_{rel} \, d\vec{v}_1 \, d\vec{v}_2 \quad ,$$

$$v_{rel} = \vec{v}_1 - \vec{v}_2 \quad . \tag{11}$$

Here, $n_i(n_j)$ and n_b denote the ion density of the i'th(j'th) species and the beam particle density, and suffixes 1 and 2 in Eq. (11) denote either thermal or beam particles, respectively. The parameters in Eqs. (8) through (11) are time dependent but are not shown explicitly. In many magnetic-confinement fusion devices reported to date where tritium is not introduced, the dominant term in Eq. (8) is the beam-thermal term $Y_{b\text{-}th}$, even if the density of the beam particles n_b is much smaller than n_i, because the D-D cross sections are still increasing steeply as the beam energy increases. Thus, the measurement of fusion reactivities in current devices provides the information of energetic ion behaviors but does not directly provide the fusion output.

Nevertheless, fusion product measurements play an important role in current devices. Neutron diagnostics should be mentioned specifically because as they are uncharged they are able to escape from the plasma container, carrying various types of information to the outside. When neutrons from a fusion device are measured, the reaction rate defined as in Eq. (8) is frequently expressed as the neutron emission rate. There have been several review articles on neutron diagnostics, such as that by Jarvis.[6] The physics and experimental observations on energetic ion behaviors were instructively reviewed by Heidbrink and Sadler.[7] One example of an energetic ion confinement study is the triton burnup, which measures the D-T reaction rate produced by confined/decelerated tritons originating from D-D fusion reactions in a deuterium plasma. Cited references are not always the first published example of each type of measurement. Further lists of publications were seen in review articles.[6,7]

The importance of fusion product measurement expands beyond the energetic ion behaviors in future fusion

devices such as ITER. Starting from individual measurement techniques, this article describes the quantities and information obtained with fusion product measurement and discusses its prospective role in future fusion experiments. Parameters that can be measured are the fusion power, the fluence on the first wall (FW), the ion temperature, the fuel isotope ratio (n_T/n_D), energetic alpha-particle density, and location and parameters of alpha-particle loss. The output fusion power is an essential parameter for the ITER project, and this can be determined from the spatially integrated neutron emission rate. Time variation and the profile of the neutron emission rate are key parameters for plasma control and operation. Tests of various types of candidate blanket will be carried out on ITER, and the neutron fluence on the FW is an inevitable key parameter for these experiments. The fuel isotope ratio and parameters related to alpha particles are important to control the fusion output and to study the new field of a self-heating plasma. These parameters often cannot be determined by a single measurement system but require a combination of two or more systems. For example, the fusion output, which should be measured by time-resolved emission monitors well calibrated onsite with high accuracy and high reliability, will be cross-checked using several detectors. Moreover, the integral of the neutron rate from a shot is checked by the total yield, as measured by the activation system. There have been several recent overviews of fusion product diagnostics[8,9] on ITER and the plasma parameters that can be measured with the various fusion product diagnostics on ITER are listed in Table I.

In this paper, we first describe the neutron time-resolved emission rate (Sec. II), and time-integrated measurement of neutron emission rate (Sec. III), followed by measurement of neutron emission profiles (Sec. IV) and energy spectra (Sec. V). Then, we describe the measurements of other fusion products, gamma rays (Sec. VI), and escaping charged fusion products (Sec. VII). Each section contains a general explanation of current systems along with some experimental results obtained using these systems. The systems on ITER are then briefly described. The measurement of fusion-produced alpha particles confined in the plasma is described in other chapters, so they are reviewed briefly in Sec. VII.

II. ABSOLUTE MEASUREMENT OF NEUTRON EMISSION RATE

II.A. Introduction to Neutron Emission Rate Measurement

The absolute measurement of neutron emission rate from the whole plasma is a very important diagnostic as a fusion power monitor in fusion experimental devices with D-T or D-T operations. A neutron emission rate of $1\ s^{-1}$ is equivalent to the fusion power of 2.86×10^{-12} W in the D-T plasma and 1.17×10^{-12} W in the D-D plasma, respectively. So, the neutron emission rate will be used as a feedback parameter for fusion output control in ITER or other burning plasma devices. On JT-60U, feedback control by the neutron emission rate has been demonstrated for optimization of operation, such as avoidance of minor disruptions or maintaining a steady-state plasma condition where the neutral beam power was modulated as an actuator.[10] In the burning plasma devices, a device aimed toward a self-sustaining reacting plasma for nuclear fusion power plants, a fusion gain of Q, which is fusion-output power divided by the input power to the plasma, is one of the most important parameters indicating reactor performance.

In fusion experiments with auxiliary heating, such as NBI, the neutron emission rate changes from 10^4–10^6 over the time scale of the fast ion slowing-down time ($\sim$100 ms). Therefore, the detector of the neutron emission rate must have a wide dynamic range and fast response time and also be immune to spurious signals from hard X-rays and gamma rays. To fulfill these two requirements simultaneously, a fast response neutron detector that selectively produces a large signal only for neutrons is used in combination of two operation modes: a pulse-counting mode and a direct current–like mode, such as the current mode. The BF_3 proportional counters, ^{3}He proportional counters, and ^{235}U fission chambers are the most commonly used neutron detectors.[11] The BF_3 and ^{3}He proportional counters utilize $^{10}\mathrm{B}(n,\alpha)^7\mathrm{Li}$ and $^3\mathrm{He}(n,p)\mathrm{T}$ reactions, respectively, and the amounts of excess energy produced through these reactions are 2.78 and 0.77 MeV, respectively. The ^{235}U fission chambers utilize the $^{235}\mathrm{U}(n,\mathrm{fission})$ reaction producing $\sim$200 MeV of energy. As the energy dependence of these reactions is proportional to $E^{-1/2}$, these detectors are more sensitive to low-energy neutrons. To detect higher-energy neutrons, these detectors are often used with moderators to slow down fast neutrons. A fission chamber is an ionization chamber with electrodes coated with fissile material such as ^{235}U or ^{238}U, and ionization of the chamber gas is caused by fission fragments produced at the electrode with kinetic energy of 50 to 200 MeV. Here, it should be noted that ^{238}U fission chambers are sensitive only to fast neutrons because the $^{238}\mathrm{U}(n,\mathrm{fission})$ reaction has a threshold of $\sim$1 MeV.

In current tokamak experiments, fission chambers are employed for neutron emission rate measurement. As the energy of background hard X-rays or gamma rays is $<$10 MeV in fusion devices, even in ITER, the fission chamber can eliminate hard X-rays or gamma rays by the conventional pulse-height discrimination technique. The typical pulse width is $<$100 ns. In low neutron flux, we can count electric pulses induced by fission events in the chamber, which is called pulse-counting mode. In high neutron flux, each electric pulse can no longer be counted because of piling up of pulses, where the average current induced by fission events can be measured (current mode). In this case, the Campbell (mean square voltage) mode[12]

TABLE I

Parameter/Technique Matrix for Fusion Product Diagnostics

Measurement System	Measurement Parameter										
	Fusion Power			Fluence on FW	Ti	n_T/n_D	Confined Alpha		Lost Alpha		Described Section
	Absolute Value	Time Variation	Profile				Integrated	Space and Time-Resolved	Image	Energy and Time-Resolved	
Microfission chambers	●	●		●							II
External neutron flux monitor	●	●		●							II
Divertor neutron flux monitor	●	●		●							II
Neutron activation system	●	+	+	+							III
Radial neutron camera	●	●	●	+							IV
Vertical neutron camera	●	●	●	+							IV
Energy-resolved detectors in camera chords	+	♦	♦	+	●						IV
Compact neutron spectrometers	+	♦	♦	+	●	●					IV
Large neutron spectrometer						●	♦				V
Lost alpha imaging camera									●	+	VII
Lost alpha probes									+	●	VII
Gamma-ray spectrometer								●			VI
Collective Thomson scattering								●			VII
Double charge exchange beam								●			VII

Note: ● = primary (technique is well suited to the measurement); ♦ = backup (technique provides similar data to the primary but has some limitations); and + = supplementary (technique can provide data that can be used to improve or check aspects of the main measurement but is not complete in itself).

is also available, where the mean square of the induced current signal is proportional to the fission event rate. The fission chamber can be operated simultaneously in pulse-counting mode, Campbell (mean square voltage) mode,[12] and current mode. As the sensitivities of these proportional counters are about 100-fold higher than that of a typical ^{235}U fission chamber of the same size,[10] BF_3 and ^{3}He proportional counters are useful for low neutron yield experiments. The gamma-ray shielding should be considered in the use of these detectors.

To determine the absolute neutron emission rate from the whole plasma, the relation of the detected signal level to it should be known accurately. As (a) the source is extended in a torus shape, (b) there are complicated structural materials that act as energy degraders and neutron absorbers between the source and detector and (c) each detector has its individual energy response, in situ calibration experiments using a neutron source inside the vacuum vessel supported by a neutron transport code such as MCNP (Monte Carlo N-Particle transport code developed at the Los Alamos National Laboratory[13]), are inevitable.

II.B. Examples of Neutron Emission Rate Measurement

Figure 2 shows the schematics of the JT-60U neutron monitor using ^{235}U and ^{238}U fission chambers.[10] The detectors are all long cylinders. The ^{235}U detector is surrounded by a 50-mm-thick polyethylene layer as a moderator and a 1-mm-thick layer of cadmium acting as a thermal neutron shield, the neutron sensitivity of which is estimated to be almost constant in the energy range of 0.55 eV to 2.5 MeV. The detectors were oriented vertically and placed just beyond the outer diameter of the toroidal field coils to reduce the effects of the magnetic fields. These fission chambers are operated in both pulse-counting mode and Campbell mode.[12] The former is suitable for low count rates of less than 10^6 count/s, while the latter are suitable for count rates higher than 10^5 count/s. Three pairs of ^{235}U and ^{238}U fission chambers are located on the torus mid-plane in JT-60U. Similar neutron emission rate diagnostics have been employed in JET (Ref. 14) and TFTR (Ref. 15).

Absolute calibration of the relation between the neutron emission rate in the whole plasma and the output of the neutron monitor is the most important problem in neutron emission rate measurements. This calibration is rather difficult because the neutron source is distributed in the plasma, which is surrounded by many complicated structures such as the FW, vacuum vessel, and both poloidal and toroidal coils. A great deal of time and effort have been devoted to neutron calibrations at many tokamaks.[16] The calibration of neutron detectors has been performed by moving a neutron source around the inside

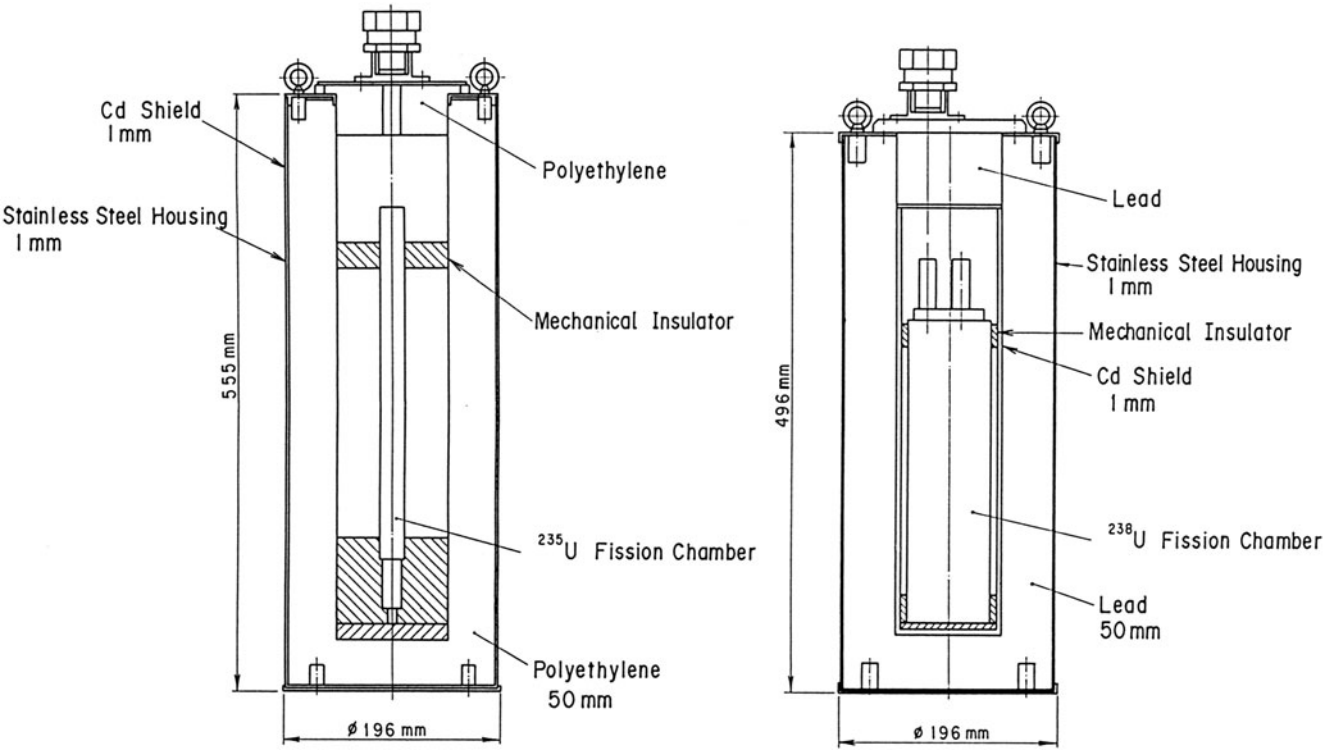

Fig. 2. Schematic diagram of the JT-60U neutron monitor using ^{235}U and ^{238}U fission chambers.

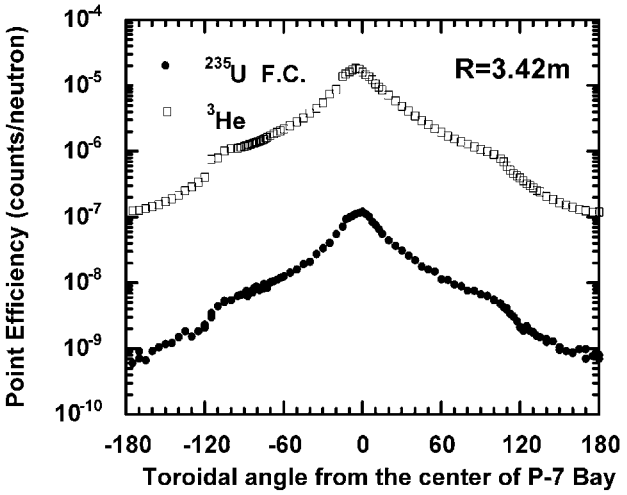

Fig. 3. Point efficiencies of ^{235}U fission chamber and ^{3}He proportional counter located at bay P-7 of JT-60U as a function of toroidal location of a ^{252}Cf neutron source.

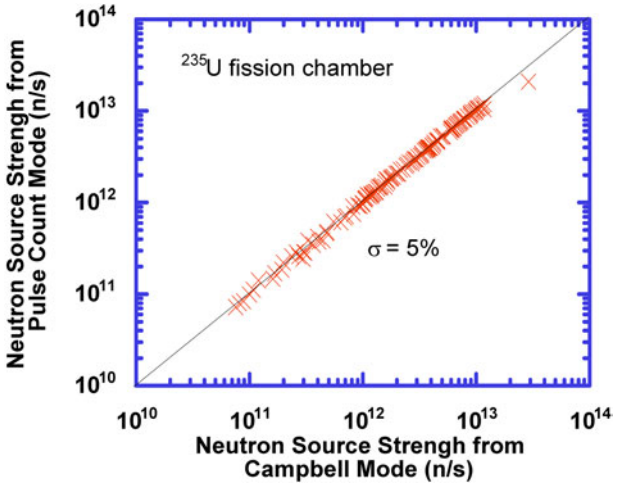

Fig. 4. Cross calibration of the ^{235}U fission chamber between pulse-counting and Campbell modes using real tokamak discharge in JT-60.

of the vessel at known positions. For D-D operation, a ^{252}Cf neutron source is typically used.[10] However, a ^{252}Cf neutron source is not suitable for D-T operations because the average energy of 2.1 MeV is much lower than 14 MeV. A compact D-T neutron generator was used for the D-T operation of TFTR (Ref. 17). Figure 3 shows the dependence of the ^{235}U fission chamber and the ^{3}He proportional counter located at bay P-7 of JT-60U as a function of toroidal location of a ^{252}Cf neutron point source. The detection efficiency of these detectors can be determined by integration of the point efficiencies obtained in the calibration experiment. In JET, the fission chambers were cross calibrated with the time-integrated neutron yield measured by the neutron activation technique (see Sec. III).

Campbell mode or current mode is employed for high neutron yield operations, such as neutral beam heating (NBH) plasma scenarios. The intensity of a ^{252}Cf source or a compact D-T neutron generator is too low to calibrate the fission chamber in current mode or Campbell mode directly. So, cross calibration of the fission chamber from pulse-counting mode to current mode or Campbell mode is necessary using real tokamak ad hoc discharges with neutron source strength in the range overlapping pulse-counting mode and current mode or Campbell mode. In the neutron emission rate measurement system using detectors of different sensitivities, cross calibration is also done between the higher and lower sensitivity detectors using the plasma as a neutron source. Figure 4 shows the result of cross calibration between pulse counting and Campbell modes using a real tokamak discharge in JT-60, where a good degree of linearity between the pulse-counting and Campbell modes was confirmed.

The neutron emission rate is also an important parameter in the transport analysis of D-D or D-T plasmas. The neutron emission rate is analyzed by a transport code[18,19] such as TRANSP or TOPICS, by using measured basic parameters such as ion and electron temperatures, and the electron density. Comparison of the calculated and measured neutron emission rates allows refinement of the input basic parameters and validates the analysis results. As described in Sec. I, for NBH plasmas, the total neutron emission rate consists of the thermonuclear, beam-plasma, and beam-beam components. These analyses provide the fraction of each component. For D-D plasmas, the fusion gain $Q_{\text{D-D}}$ can be used to predict equivalent fusion gain, $Q_{\text{D-T}}$, in a D-T plasma where plasma parameters such as the temperature and density are taken from the set of D-D parameters. Figure 5 shows the time evolutions of the neutron emission rate and the stored energy for a high β_p H-mode plasma of JT-60U compared with the calculated values by the TOPICS code. The calculated values agreed well with the measured neutron emission rate and stored energy. Fractions of the thermal-thermal reactions, the beam-thermal, and beam-beam reactions were 45, 45, and 10%, respectively, at 6.27 s. At the same time, the equivalent $Q_{\text{D-T}}$ was estimated to be 0.61 (Ref. 20). Many comparisons of this type are reviewed in Ref. 7.

The neutron emission rate measurement is also useful to study the behavior of energetic particles. Slowing down and confinement properties of NBI fast particles can be investigated by the decay time constant of the neutron emission rate after the short-pulsed NBI, which is called an NB-blip experiment.[21] The D-D reaction cross-section $\sigma_{\text{D-D}}$ is approximately proportional to $E_b^{1.8}$ in the energy range of 50 to 100 keV, where E_b and v_b are the

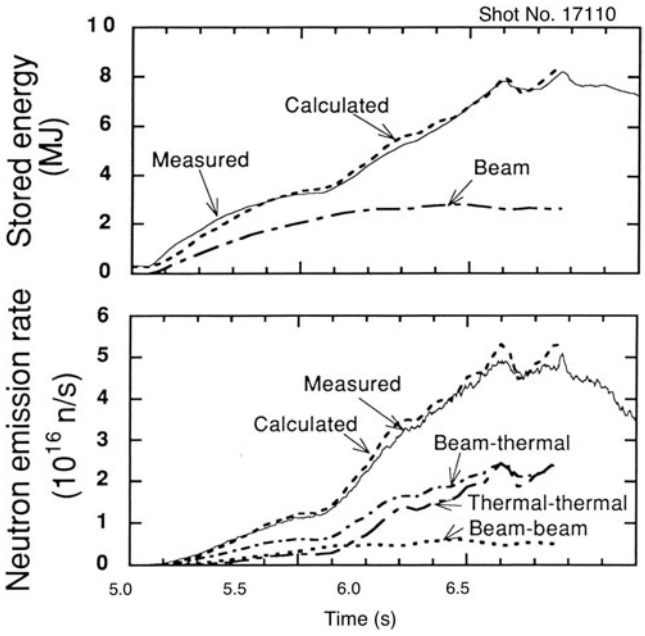

Fig. 5. Comparison of measurements and calculations from TOPICS code for the stored energy and neutron emission rate on the JT-60U high βp plasma.

energy and velocity of beam particles, respectively. Thus, the beam-thermal reactivity has a dependence of $E_b^{1.8} \times v_b$ or $E_b^{2.3}$. The neutron decay time t_n can be represented by $1/t_n = 1/t_c + 2.3/t_s$, where t_c and t_s are the fast particle confinement time and the slowing-down time, respectively. If the slowing-down process of fast particles is assumed to be classical, the confinement time of fast particles can be derived from the neutron decay time.

Tritons of 1.0 MeV are produced in the $d(d,p)t$ reaction at approximately the same rate as the 2.5-MeV neutrons from the $d(d,n)^3$He reaction. The behavior of 1-MeV tritons produced in a D-D plasma can be used to predict 3.5-MeV alpha-particle behavior produced in a D-T plasma because 1-MeV tritons and 3.5-MeV alpha particles have similar kinematic properties, such as Larmor radius and precession frequency. The 1-MeV tritons slow down and may undergo a D-T fusion reaction, emitting 14-MeV neutrons (triton burnup; recent work is introduced in Ref. 7, more description in Sec. V.A). The confinement and slowing down of the fast tritons can be investigated by measuring the 14- and the 2.5-MeV neutron production rates. Time-resolved 14-MeV neutron measurements were performed by using a silicon diode in JET (Ref. 22), TFTR (Ref. 23), and JT-60U (Ref. 24). The count rate of the silicon diode was limited to <100 kHz. Furthermore, the silicon diode can be damaged easily by neutron irradiation less than $\sim 10^{12}$ cm^{-2}, which corresponds to neutron fluence at the detector for only about 100 high neutron yield discharges.[6] Time-resolved triton burnup measurements have been performed using a new type 14-MeV neutron detector based on scintillating fibers[25] with a good time response at JT-60U. From the decay curve of the 14-MeV neutron emission rate measured by the scintillating fiber detector after NBI, the diffusivity of fast tritons was evaluated to be 0.05 to 0.15 m^2/s in JT-60U.

II.C. Emission Rate Measurement Systems of ITER

As the neutron emission rate changes in ITER over the order of 10^{13}, from 10^8 n/s (typical D-D neutron calibration source) to 5×10^{20} n/s (expected highest fusion output), a combination of several neutron flux monitors, internal flux monitors, external flux monitors, and diverter flux monitors, each again consisting of several detectors of different sensitivity, is proposed for the measurement. In addition, the neutron emission rate can be derived from the neutron emission profile measurements employing a tomographic inversion technique (described in Sec. IV) and cross checked with the results obtained from activation systems.

As ITER has a thick blanket and vacuum vessel, neutron detectors outside the vacuum vessel may not measure the neutron emission with sufficient accuracy. The internal flux monitor using microfission chambers, which are pencil-sized gas counters with fissile material inside, was proposed. At the beginning of the design work, it was planned that microfission chambers would be installed between the vacuum vessel and the shielding blanket module at several poloidal angles to reduce the effects of the plasma position and neutron emission profile on the total neutron emission rate.[26] Recently, it was found by neutron Monte Carlo calculations that the average output of the microfission chambers at two poloidal locations shown in Fig. 6, together with other neutron measurement systems, is insensitive to the changes in the plasma position and the neutron source profile. The sheath of the microfission chamber will be welded to the vacuum vessel, which is cooled by water coolant, and will be cooled by heat conduction.

In the in-vessel neutron monitor, microfission chambers must be operated in a high vacuum, high magnetic field, and high radiation environment inside the vacuum vessel. A prototype microfission chamber with 12-mg UO_2 has been developed for the ITER to check the reliability under ITER conditions, such as high vacuum, neutron and gamma radiation, high temperature, and mechanical vibration.[27] In addition, the burnup rate of ^{235}U was estimated and the sensitivity change was only 0.1% behind blankets for the ITER lifetime, which is equivalent to 0.5 GW per year. Thus, the ^{235}U chambers can be used without replacement during the ITER lifetime. From these tests and estimations, a favorable evaluation of the applicability of the microfission chamber to ITER was obtained. Using a set consisting of a ^{235}U microfission chamber with 12-mg UO_2 and a fissile-material–free "blank" detector and by employing both

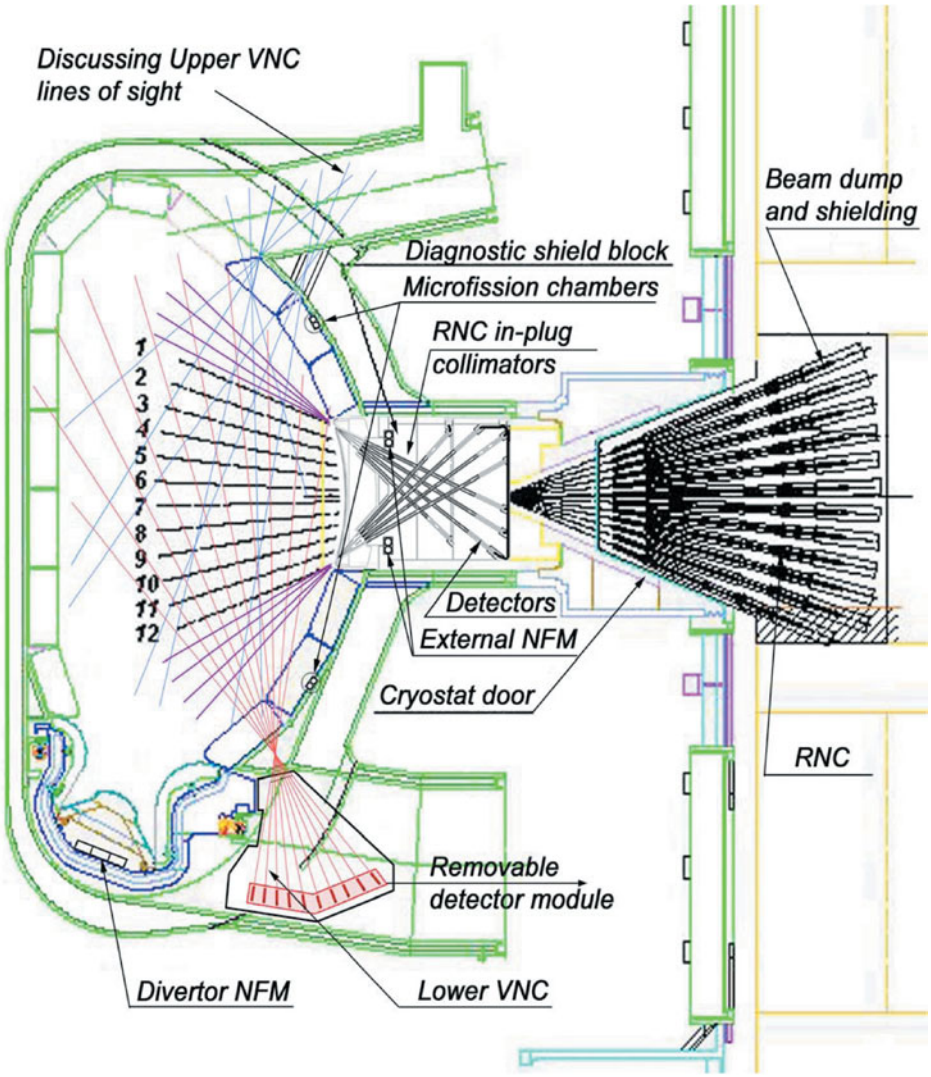

Fig. 6. Arrangement of ITER neutron diagnostic systems integrated from several toroidal plans. The 2-D neutron source strength and energy distribution measurements in ITER with the required temporal (1 ms for source strength and 0.1 s for energy distribution) and spatial resolutions (a/10) can be made by joint application of RNC including compact in-plug collimators and VNC (Ref. 9).

pulse-counting and Campbell modes in the electronics, the ITER requirement of 10^7 dynamic range to the maximum ITER operation with temporal resolution of 1 ms will be accomplished without contamination by noise arising from gamma rays, etc.[27]

A conventional neutron monitor installed outside the vacuum vessel is also considered in ITER. However, neutron flux outside the vacuum vessel is not sufficient to obtain the required accuracy. Several external flux monitor conceptual designs have been proposed using fission chambers of normal size to be installed in the ITER equatorial port.[6,28] Asai et al. investigated a moderator material for the ^{235}U fission chamber with the aim of obtaining a flat energy response of the detectors.[28] Here, graphite and beryllium with a ratio of Be/C = 0.25 were employed as moderator materials, which are stable in ITER relevant temperature in an equatorial port. Based on the neutronics calculations, a fission chamber with 200 mg of ^{235}U was adopted for the neutron flux monitor. Three detectors were mounted in a stainless steel housing with moderation material. Two assembly blocks will be installed in an equatorial port; one for D-D and calibration operation, and another for D-T operation. The assembly block for D-D operation and the calibration experiment was installed just outside the port plug in the equatorial port. The assembly block for the D-T operation was proposed to be installed just behind the shielding block in the port. Another concept uses integration of detector blocks consisting of a set of ^{235}U and ^{238}U fission chambers of different sensitivity into the stainless steel + water

shielding modules of the limiter moving the mechanism inside equatorial ports #8 and #17 (Ref. 9).

An in situ calibration experiment of several sensitive neutron monitors is planned using a ^{252}Cf source and a compact neutron generator inside the vacuum vessel before the deuterium operation.[6,8,9,29] Careful characterization of the neutron generator must be made with regard to the emission strength, directionality, and energy spectrum before the calibration experiment. Furthermore, detailed neutron transport analysis, using a simulation code such as MCNP, and cross calibration for less sensitive monitors and/or calibration of Campbell/current mode using the ITER plasma over a wide dynamic range are necessary.

III. NEUTRON ACTIVATION MEASUREMENT

III.A. Neutron Activation

The neutron activation system provides time-integrated measurements of the total neutron yield with high degree of accuracy using well-known neutron reaction cross sections. If the irradiation point is installed near the plasma, the relation between the neutron emission rate in the whole plasma and the neutron flux at the irradiation point should be calibrated by neutron Monte Carlo calculation with precise machine modeling. Here, the neutron transport itself should be studied intensively, and a benchmark study is needed.

The primary goals of the neutron activation system are to maintain a robust relative measure of fusion energy production with stability and a wide dynamic range, to enable accurate absolute calibration of fusion power, and to provide a flexible system for materials testing. Fluxes of D-D and D-T neutrons can be measured easily with several foils with different threshold energy reactions[6] as shown in Table II. From the ratio of D-D and D-T neutron fluxes, the triton burnup ratio in D-D plasmas and the deuterium/tritium fuel ratio (n_d/n_t) in D-T plasmas can be derived in principle. A sophisticated multifoil activation technique using an unfolding code, such as SAND-II, can provide a neutron energy spectrum at the irradiation point,[30] which is useful for testing of the neutron transport methodology from the viewpoint of fusion neutronics.[31] In addition, pneumatic sample transfer systems can be used for material irradiation tests for diagnostic and development of other components.

III.B. Examples of Neutron Activation Measurement

The neutron activation method using solid samples is used for accurate measurement of the neutron yield in many fusion devices without temporal resolution. At current large tokamaks, pneumatic operated sample transfer systems are employed using polyethylene capsules. JET and TFTR have multiple irradiation positions[32,33] with different poloidal locations, while JT-60U has a single position[34] of the irradiation end in a horizontal port. Figure 7 shows poloidal locations of the irradiation end on JET. There is mirror symmetry in the horizontal midplane. The effect of the vertical plasma displacement on the total neutron yield can be corrected automatically by averaging the results obtained from vertically opposed pairs of irradiation positions against the midplane. A capsule with sample foils can be transferred to the selected irradiation end via a "carousel" switching system from a capsule loader in the gamma-ray counting station before a plasma shot. After the plasma shot, each capsule returns to the gamma-ray counting station by the pneumatic transfer system. Gamma rays from the activated samples are measured with a germanium detector or NaI scintillation detector. In the case of fissile samples, such as ^{232}Th or ^{238}U, delayed neutrons from the irradiated samples are measured with high-sensitivity neutron detectors, such as ^{3}He or BF_3 proportional counters.

TABLE II

Major Reactions Used for Activation Measurements for D-D and D-T Plasmas*

Reaction	Threshold Energy (MeV)	Half-Life
For D-D neutrons		
$^{58}\mathrm{Ni}(n,p)^{58}\mathrm{Co}$	1.0	70.82 day
$^{64}\mathrm{Zn}(n,p)^{64}\mathrm{Cu}$	1.8	12.70 h
$^{115}\mathrm{In}(n,n')^{115m}\mathrm{In}$	0.5	4.486 h
$^{232}\mathrm{Th}(n,f)$F.P.	1.2	~1 min
$^{238}\mathrm{U}(n,f)$F.P.	1.0	~1 min
For D-T neutrons		
$^{27}\mathrm{Al}(n,p)^{27}\mathrm{Mg}$	2.6	9.458 min
$^{28}\mathrm{Si}(n,p)^{28}\mathrm{Al}$	5.0	2.25 min
$^{56}\mathrm{Fe}(n,p)^{56}\mathrm{Mn}$	4.5	2.577 h
$^{63}\mathrm{Cu}(n,2n)^{62}\mathrm{Cu}$	10.9	9.74 min
$^{93}\mathrm{Nb}(n,2n)^{92m}\mathrm{Nb}$	9.0	10.25 day

*See Ref. 6.

III.C. Neutron Activation Systems of ITER

ITER has two types of the neutron irradiation system: a conventional foil activation measurement using a pneumatic capsule transfer system and a flowing water activation measurement based on the $^{16}\mathrm{O}(n,p)^{16}\mathrm{N}$ reaction with reasonable temporal resolution.

The present design of the foil activation system provides irradiation stations at two upper ports, one equatorial port, and several positions on the ITER vacuum vessel wall.[35] Figure 8 shows a schematic plan view of the routing of pneumatic transfer lines from the irradiation ends between shielding blanket modules to a

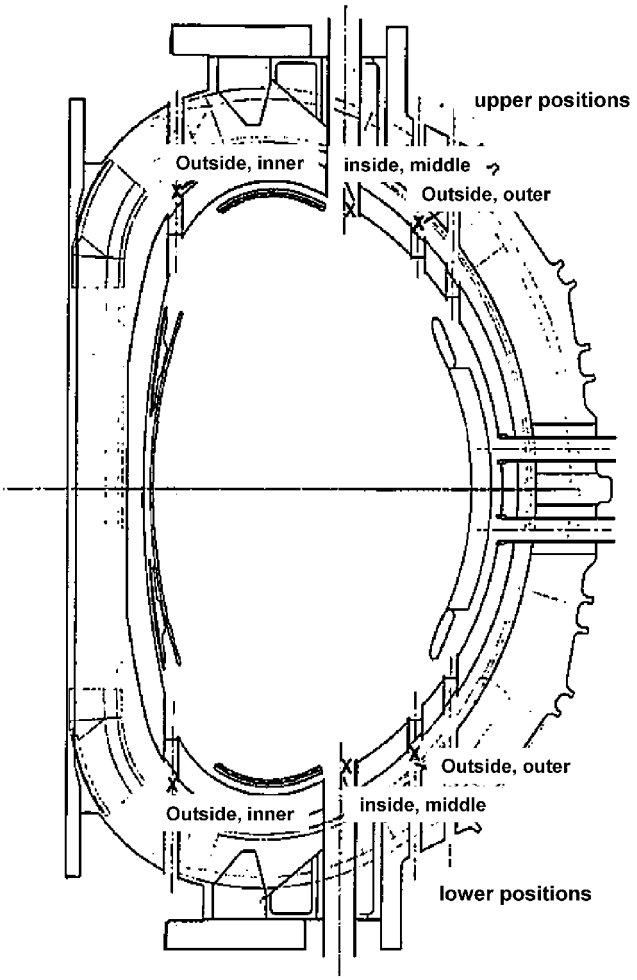

Fig. 7. Poloidal location of the irradiation ends on JET (Ref. 6).

carousel pneumatic switching system, and then to counting stations and a loader in the tokamak building. The coaxial pneumatic transport tubes will have outer and inner diameters of 2 and 1.1 cm, respectively, and will carry capsules 1 cm in diameter. The configuration of the coaxial design at the irradiation end allows the return air to be transmitted to the inner tube. Every necessary turn on the route should have a radius of curvature greater than 10 cm. Helium will be used as a pneumatic propellant, and the airlock device separates the primary loops containing the irradiation stations from the secondary loops of the capsule loader. The activated samples are unloaded at the pneumatic switchyard for transfer to the counting station. Appropriate locations of the loader and counting station are currently under investigation. Activation of irradiated samples will be about 100 μCi (3.7×10^6 Bq) for modestly safe handling. Candidate materials are Fe, Al, and Ti foils that appear to allow for reasonable sensitivity without creating a source that is too intense. Si could be useful at low power. These samples can provide a neutron source strength of 10^{17} to 10^{21} n/s with accuracy of 10% every few 100 s.

The neutron activation system with fluid flow[36] consists of a closed water loop laid between the FW/blanket region and a remote low-background location, as shown in Fig. 9. It is possible to determine the D-T neutron yield continuously by measuring the gamma rays from ^{16}N with a gamma-ray detector placed beside the water loop. The activated water will remain in a reservoir tank to reduce the activity and will be transferred again to the FW/blanket region. The ^{16}O(n, p) ^{16}N reaction has a high threshold energy of 10.24 MeV. Therefore, the water activation is sensitive for almost nonscattered neutrons. The ^{16}N nucleus emits 6.13 (68.8%) and 7.12 (4.7%) MeV gamma rays with a half-life of 7.13 s. The irradiation end should be as close to the plasma as possible. The original proposal was for the irradiation end to be installed in the filler blanket. As it is difficult from an engineering viewpoint to pass the water tubes through the vacuum vessels, filler modules beside the port plug will be used for the irradiation ends where the tube will be able to run under the port plug with other cooling pipes of the plug. The upper port and equatorial port are envisaged for the water flow system. The gamma-ray counting station, in the pit area or heat transfer system vault ~20 m from the irradiation end, consists of a pair of bismuth germanium oxygen (BGO) scintillation detectors with different geometric efficiencies. Based on the results of dedicated research and development on a prototype water loop using the D-T neutron source of the Fusion Neutronics Source[37] (FNS) at the Japan Atomic Energy Agency (JAEA), the present system can measure the neutron source strength of 10^{16} to 10^{21} n/s (corresponding to 50 kW to 1000 MW) with time resolution of 100 ms or less. A further development of this system where the Cherenkov radiation from the irradiated portion is relayed out of a port plug is currently under assessment.[38]

Both systems can be calibrated by Monte Carlo calculations with precise three-dimensional modeling. In addition, those systems will be calibrated experimentally by scanning a compact neutron generator within ±30 deg in toroidal angle, which will result in accuracy of 10%. The encapsulated foil system will have better accuracy when the fusion power is stable, while the water flow system responds quickly to changes in power. Taken together, these systems will provide a robust, independently calibrated measurement.

IV. MEASUREMENT OF NEUTRON EMISSION PROFILES

IV.A. Introduction to Neutron Emission Profiles

As mentioned above, the neutron source in a fusion plasma consists of a thermonuclear component and a component produced by fast deuterons and tritons. The

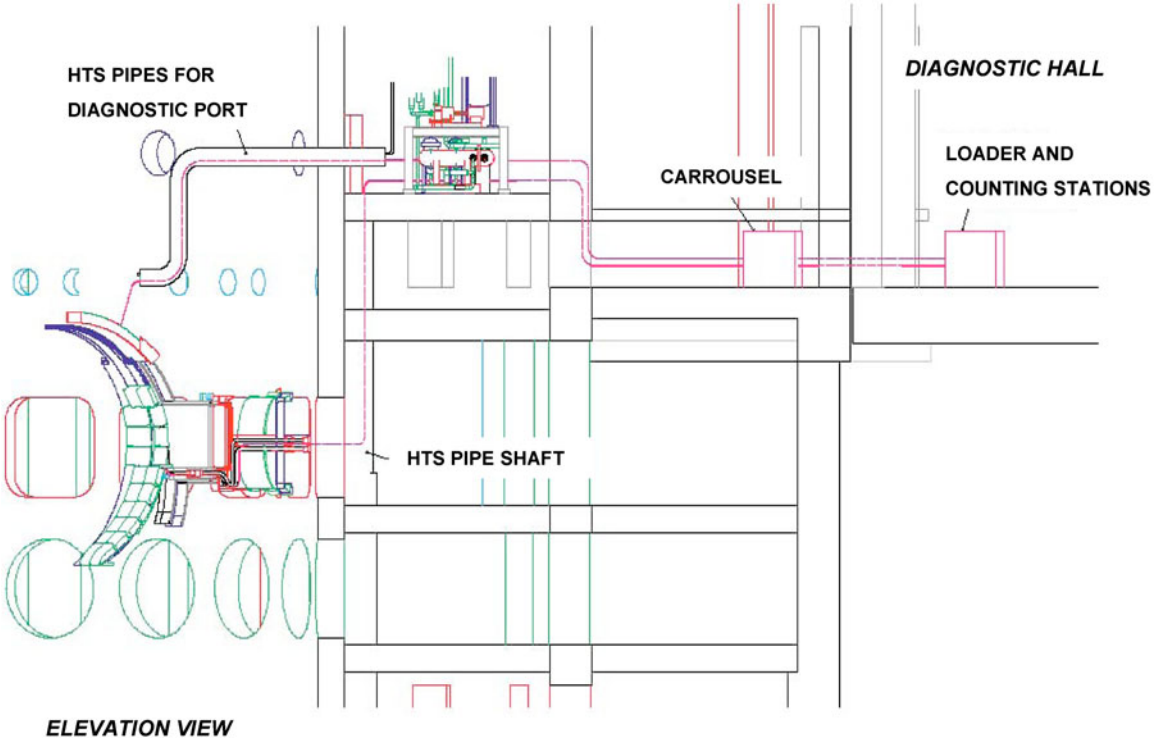

Fig. 8. Schematic plan view of the routing of pneumatic transfer lines from [CW1] between shielding blanket modules, to a carousel pneumatic switching system, and then to counting stations and a loader in the tokamak building.

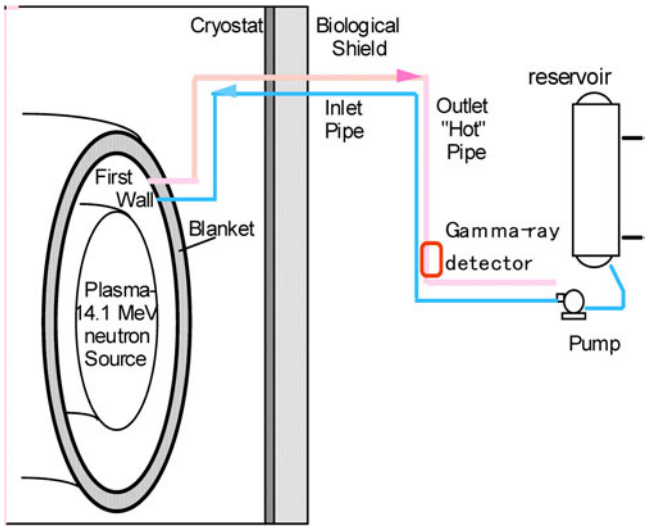

Fig. 9. Concept of neutron activation system with fluid flow.

thermonuclear neutron source profile is usually a function of the magnetic surfaces, but this is not true for the neutron source component related to fast ions. Their behavior in reactor plasma is crucially important, especially in driven regimes approaching the "ignition" (see Sec. I). Measurements of spatial and energy distributions of fast confined deuterons and tritons in future reactor plasma experiments will be difficult for a number of reasons but are very important for optimization of NBI and ICRF heating and current drives. Neutron source profile measurement is the principal method for the measurement of fast deuteron and triton distributions. Because of nonuniformity of fast beam and ICRF-driven deuteron and triton distributions on magnetic surfaces, the two-dimensional (2-D) neutron source profile measurements are required. This requirement is becoming stronger for optimization of the method of ignition for the fast ion-driven advance tokamak discharge scenario and plasma influenced by magnetohydrodynamic (MHD) instabilities.

IV.B. Neutron Emission Profile Measurement Systems and Detectors

The primary function of a neutron profile monitor is to measure the neutron emissivity over a poloidal cross section of the plasma using line-integrated measurements recorded by neutron detectors viewing the plasma along a number of chords (lines of sight). To avoid contamination of the scattering component, it is important to use a detector that is insensitive to low-energy neutrons. It can also be evaluated by scanning an intense neutron generator across an aperture in two directions or by the

"jog shot" procedure, where the plasma is shifted quickly in the major radius.[39]

Knowledge of the absolute detection efficiency of the system enables us to obtain the total instantaneous neutron yield from the tokamak independently supplementing the results obtained using other techniques, such as neutron activation or neutron flux monitors. Combining many of the features of the other neutron diagnostic, a well-designed neutron profile monitor is potentially the most important of its range. However, there are several instrumental limitations that prevent it displacing the other diagnostics:

1. The dynamic range is usually limited to a few orders of magnitude.

2. Achievement of an accurate (better than 10%) absolute global neutron detection efficiency for the instrument is difficult.

3. The energy resolution of the existing detectors is insufficient to obtain the ion temperature profile.

4. Detectors with good separation from gamma-ray signals must be provided.

Typically, a profile monitor consists of one or more massive radiation shields with embedded multiple channels through which the neutron detectors view the plasma. In practice the instrument must be placed as close as possible to the tokamak to obtain the fullest possible view of the plasma. The degree of shielding to be provided will depend on the sensitivity of the selected neutron detectors to gamma radiation. Paraffin wax (high hydrogen content) loaded with lithium to absorb the neutrons without creating energetic gamma rays may be a suitable material for shielding from background neutron radiation. However, such shields typically have little effect on the background gamma radiation. The most practical shielding material is therefore boron-loaded concrete, which can be of a high-density type if space is limited.

The detection efficiency is affected not only by structural material lying across the lines of sight but also by (a) scattering of neutrons in the collimation channels and transmission through substantial thicknesses of the shield material; (b) neutron cross talk, i.e., neutron collimated in one channel but then detected in the adjacent channel due to scattering; and (c) backscattering, i.e., neutrons impinging on the inboard vessel and then scattered back into the collimating channel. The most direct experimental method to determine the detection efficiency is the use of a calibration source placed inside the tokamak (in situ calibration procedure) as mentioned above. However, this is rather difficult in practice because of the need for a strong source. Therefore, a computational procedure using a neutron transport code[13] is required to support or even substitute for in situ calibration, and the neutronic calculations play a key role in the commissioning and operation of a neutron profile monitor.[31,40]

Organic scintillators are mainly used as neutron detectors because of their good time resolution and well-known efficiency.[41] However, as mentioned above, such detectors are sensitive not only to neutrons but also to gamma emission.[42] To distinguish neutron and gamma signals, additional electronics for discriminating gamma radiation are necessary.

All large tokamak devices, such as TFTR, JET, and JT-60U, have installed neutron profile monitors. These three instruments utilize different detectors as appropriate to their different geometrical arrangements and consequential problems.

IV.C. Profile Monitors of Present Machines

IV.C.1. TFTR Multichannel Profile Monitor

Although TFTR was shut down in 1997, it is worthwhile giving brief descriptions of all these instruments to illustrate the possible design solutions for future plasma devices. Figure 10 shows the TFTR profile monitor or multicollimator array,[43] comprised of ten vertical collimators, each providing lines of sight through the plasma that enter and leave the vacuum vessel through recessed thin vacuum windows. The spacing of the chords ranged from 14 to 30 cm for the 83-cm minor radius of the machine vacuum vessel. The flight tubes leading from TFTR to the neutron detectors located 6.3 m below the torus midplane were encapsulated with 80 tons of lead, polyethylene, and concrete blocks. This design allowed minimization of the scattering of neutrons into the lines of sight of the detectors. The TFTR plasmas were circular, so that a single viewing array was fully sufficient.

An attractive feature of the TFTR multicollimator array was that it was provided with two large detector regions in which a variety of different detector types could be investigated. As the detected flux of scattered neutrons was very small, it was not necessary to employ neutron detectors with good energy resolution to discriminate between virgin neutrons coming directly from the plasma against a background of scattered neutrons. The detector[44] NE451 was selected for D-D neutrons utilizing an arrangement of concentric rings of ZnS(Ag) scintillator crystals and clear plastic. The scintillators were coupled to a Hamamatsu R239 photomultiplier tube (PMT), which was operated in the pulse-counting mode. These detectors have been calibrated in situ using a ^{252}Cf neutron source located inside the tokamak vacuum vessel.[43] The main advantage of NE451 is its insensitivity to gamma radiation, and it has a threshold $\sim$1 MeV and can discriminate against most scattered neutrons. The signal amplitude spectrum from monoenergetic neutron detectors falls monotonically with pulse height, and events due to 2.5-MeV neutrons are not intrinsically distinguishable from those due to 14-MeV neutrons. However, the signal rate due to 14-MeV neutrons from triton burnup for D-D plasmas is generally negligible in comparison

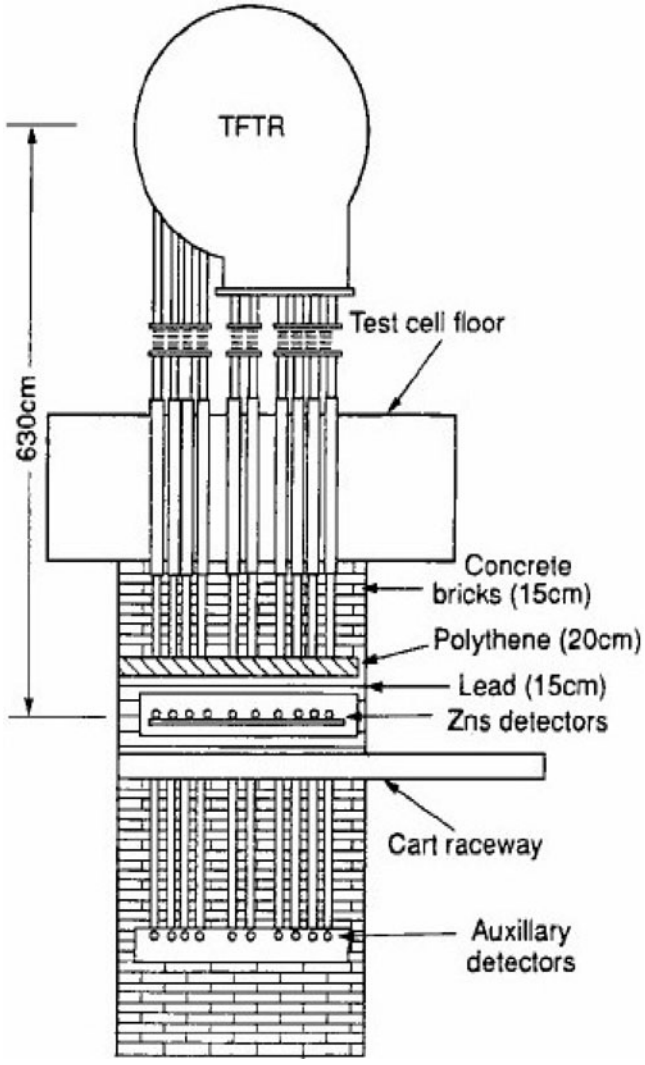

Fig. 10. Elevation view of the TFTR multichannel neutron collimator components and associated shielding.

with the D-D signal rate (typically less than 2%). The NE451 detector is suitable for D-T operation although the detection efficiency is likely to be too high. There are several approaches to resolve this problem. One proposed solution was to develop a wafer detector using a thin ZnS layer.[45] Another solution was to operate detectors in the current mode.[46,47] Adjustment to the bias allowed operation during both D-D and D-T plasmas to give dynamic range of at least 300 to 1000.

IV.C.2. JT-60U Neutron Profile Monitor

The JT-60U neutron emission profile monitor contains a single six-channel collimator array viewing the poloidal cross section through the plasma[48] as shown in Fig. 11. The line of sight of each collimator channel is constrained by the space available in the JT-60U torus

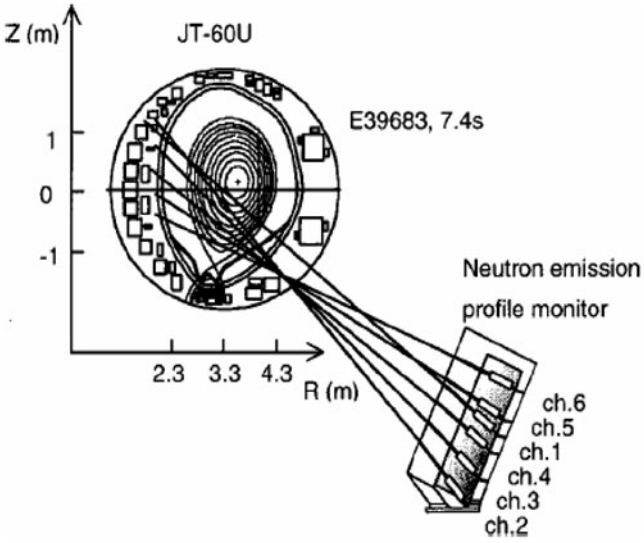

Fig. 11. Illustration of the JT-60U neutron profile monitor and its collimation geometry. The line-of-sight chords show the viewing poloidal cross section of the plasma.

hall. As illustrated in Fig. 11, one of the sight lines of the six-channel collimator passes through the vessel center ($R = 3.3$ m, $z = 0$ m) where the other chords are viewing the plasma below the middle plane.

The polyethylene assemblies are used to shield the detectors against scattered neutrons. Lead shielding surrounding the detector box reduces the gamma-ray flux generated by the neutrons incident to polyethylene and the gamma rays scattered from the external structure of the JT-60U device. The housing of the neutron detector is also surrounded by soft magnetic iron to remove the influence of the magnetic field. Each collimator tube is 30 mm in diameter and 800 mm in length providing a spatial resolution of ~200 mm at $R = 3.3$ m. The collimator array design also allows changing the aperture size up to 10 mm depending on the experimental conditions.

The neutron detector utilized in this instrument is a stilbene organic crystal scintillator with a neutron-gamma pulse-shape discrimination (PSD) circuit. A stilbene crystal is used as the scintillator material, which has excellent PSD properties,[49] and allows discrimination between scintillation by charged particles induced by neutrons and electrons induced by gamma rays. The primary calibration and gamma discrimination properties of these detectors were checked using gamma sources (^{137}Cs, ^{22}Na, and ^{60}Co) and a ^{252}Cf neutron source. The absolute neutron detection efficiency for one of the stilbene neutron detectors was determined on a 2.5-MeV neutron beam in FNS. The absolute neutron efficiency was $\sim 5.6 \times 10^{-2}$ per incident neutron for the threshold energy of 1 MeV. In addition, relative efficiencies of six stilbene neutron detectors were checked using the ^{252}Cf neutron source under the same conditions.

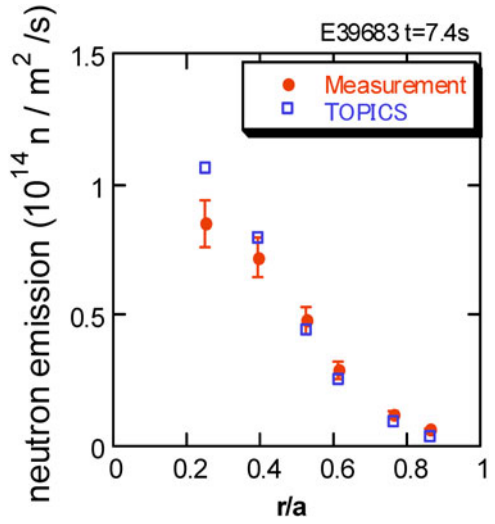

Fig. 12. An example of the profile of line-integrated neutron emission from JT-60U. Circles show the results measured in one discharge using the stilbene neutron detector; squares show the results calculated by the TOPICS code.

The system of neutron emission profile measurement was applied to deuterium experiments of JT-60U. The line-integrated total neutron signal along each sight line calculated by the TOPICS code[19] is shown in Fig. 12. Although there is 30% error in the innermost channel between measurement and calculation, there is agreement within 10% error in the other channels.

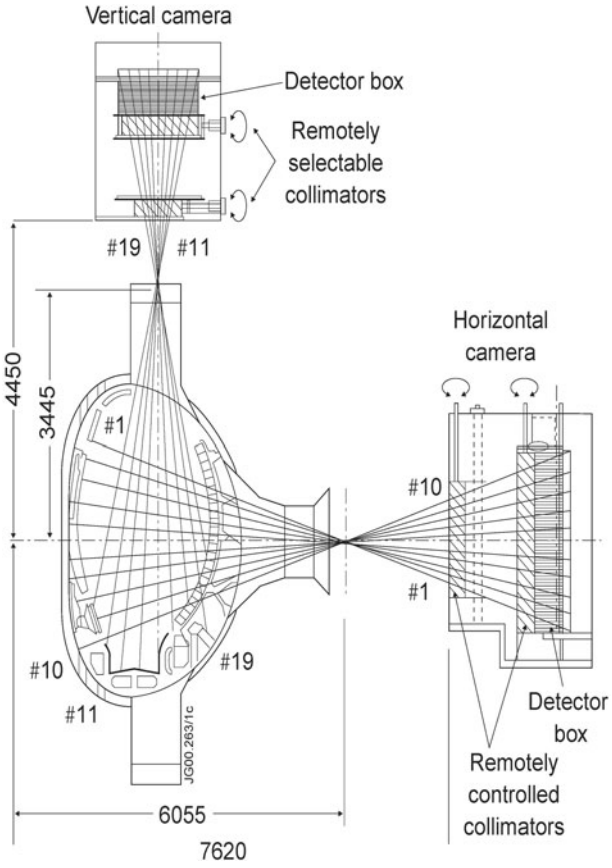

Fig. 13. Schematic view of JET neutron profile monitor.

IV.C.3. JET Neutron Emission Profile Monitor

The JET neutron profile monitor is a unique instrument among diagnostic systems available at large fusion devices. The solution adopted in JET for imaging of the noncircular plasma neutron source is to use two fan-like multicollimator detector arrays,[50,51] as illustrated in Fig. 13. A nine-channel camera is positioned above the vertical port to view downward through the plasma (vertical camera), while a ten-channel assembly views horizontally from the side (horizontal camera). The collimation can be remotely adjusted by use of two pairs of rotatable steel cylinders (a choice of two aperture sizes). The size of the collimation can modify the count rates in the detectors by a factor of 20[40].

All of the detectors view the vessel walls and machine structure, and therefore the separation of wall-scattered and virgin neutrons is essential. This can be accomplished only through energy discrimination. Each channel is equipped with a set of three different detectors: (a) a NE213 liquid organic scintillator with PSD electronics for simultaneous measurement of 2.5 MeV D-D neutrons, 14-MeV D-T neutrons, and gamma rays; (b) a BC418 (Bicron) plastic scintillation detector for measurement of 14-MeV D-T neutrons; and (c) a CsI(Tl) photodiode for measuring the fast-electron bremsstrahlung and gamma emission in the range between 0.2 and 6 MeV. Each NE213 detector-photomultiplier unit is equipped with two PSD units allowing neutrons to be separated from gamma rays and providing the necessary energy discrimination. One PSD unit is tuned for D-D neutrons and the other is tuned for D-T neutrons, so that D-D neutrons and D-T neutrons can be recorded separately. Typically, the energy band uses the thresholds set to select proton recoil events falling in the neutron energy band from 1.8 to 3.5 MeV for D-D neutrons and from 7 to ~17 MeV for D-T neutrons. The setting is controlled by recording the count rates from a ^{22}Na gamma source mounted within the scintillator. The Bicron scintillators are located in front of the NE213 scintillators and are coupled to PMTs via a light guide. They are sufficiently small and therefore relatively insensitive to gamma rays with $E\gamma < 10$ MeV. Up to four lower-energy detection thresholds could be set for each Bicron detector providing several neutron signals with different sensitivity. The detection efficiencies for each of the 19 channels (and for both D-D and D-T plasmas) are determined computationally and by

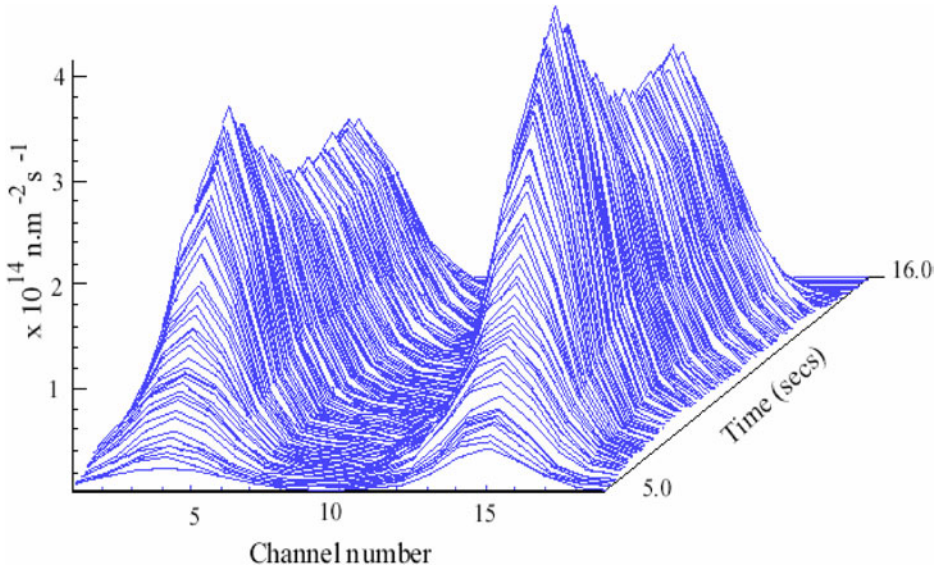

Fig. 14. Time-resolved 2-D representation of the line-integrated neutron emission recorded with the 19-channel neutron profile monitor for JET discharge #50623.

taking into account accelerator-based absolute calibrations of the scintillation detectors.[52]

The JET profile monitor allows 2-D images to be obtained from the plasma neutron emission. Typical line-integrated neutron emission measured with a JET instrument for a deuterium discharge is illustrated in Fig. 14. The JET instrument also complements activation systems and neutron flux monitors, providing an independent estimate of the absolute neutron yield from the plasma[53] and has played a key role in the 2003 Trace Tritium campaign at JET, in particular for studies on tritium transport,[54] fuel ratio,[55] and heating scenario.[56]

As mentioned above, the JET neutron profile monitor is also equipped with CsI(Tl) gamma detectors. Thus, it also acts as a gamma-ray profile monitor, as illustrated in Sec. IV.

Tomographic deconvolution of the line-integrated measurements can also be carried out to obtain a 2-D mapping of the neutron emission strength. The plasma coverage by neutron profile arrays is adequate for neutron tomography, although the spatial resolution is poor (neighboring channels are 15 to 20 cm apart and have a width of ~7 cm as they pass near the plasma center). The 2-D NEUTMO computer code was first used at JET for tomography reconstruction of neutron emissivity. This code employs a hybrid pixel/analytic algorithm, which involves poloidal Fourier analysis and radial Abel inversion.[57,58] Later, other tomography techniques, including constrained optimization, have been used successfully at JET (Ref. 59). The full power of this method is illustrated in Fig. 15 for a JET shot with the introduction of a trace amount ($n_T/n_D < 5\%$) of tritium into a D-D plasma. This discharge was characterized by the presence of a current hole, a region of negligible current in the core of the plasma with strong reverse shear. The current-hole effect on the fast particle distribution was investigated using NBI tritons as test particles and monitoring their spatial and temporal evolution with neutron cameras. The results of the reconstruction are shown in Fig. 15 for the four conditions studied. In the case of on-axis injection into a monotonic current profile, the emission peaked on the plasma axis. For injection into a current-hole plasma, there is a clear shift in the emission in the radially outward direction. For both the off-axis injection cases, the neutron emission is shifted slightly toward the inner major radius side of the plasma axis.[60] The minimum Fisher regularization method is currently under development at JET, and its potential is being assessed as a new tool to study both the 2-D spatial distribution of neutron emission and neutron spectral deconvolution.[61,62] This new approach is extremely useful for observing dynamic processes such as tritium diffusion into the plasma.[63]

IV.D. Profile Monitors of ITER

The necessity of 2-D neutron profile measurements in ITER is determined by the requirement of total neutron strength measurements with accuracy of 10% and also by the necessity of NBI and ICRF heating and current drive profile optimization. The necessity of 2-D neutron profile measurements in ITER arises from the fact that, due to fast ion components, the neutron source profile will not be constant on magnetic surfaces, especially during ion cyclotron resonance heating (ICRH), NBI, sawtooth oscillations, excitation of Alfven eigenmodes,[7] and in advanced tokamak regimes with strongly negative

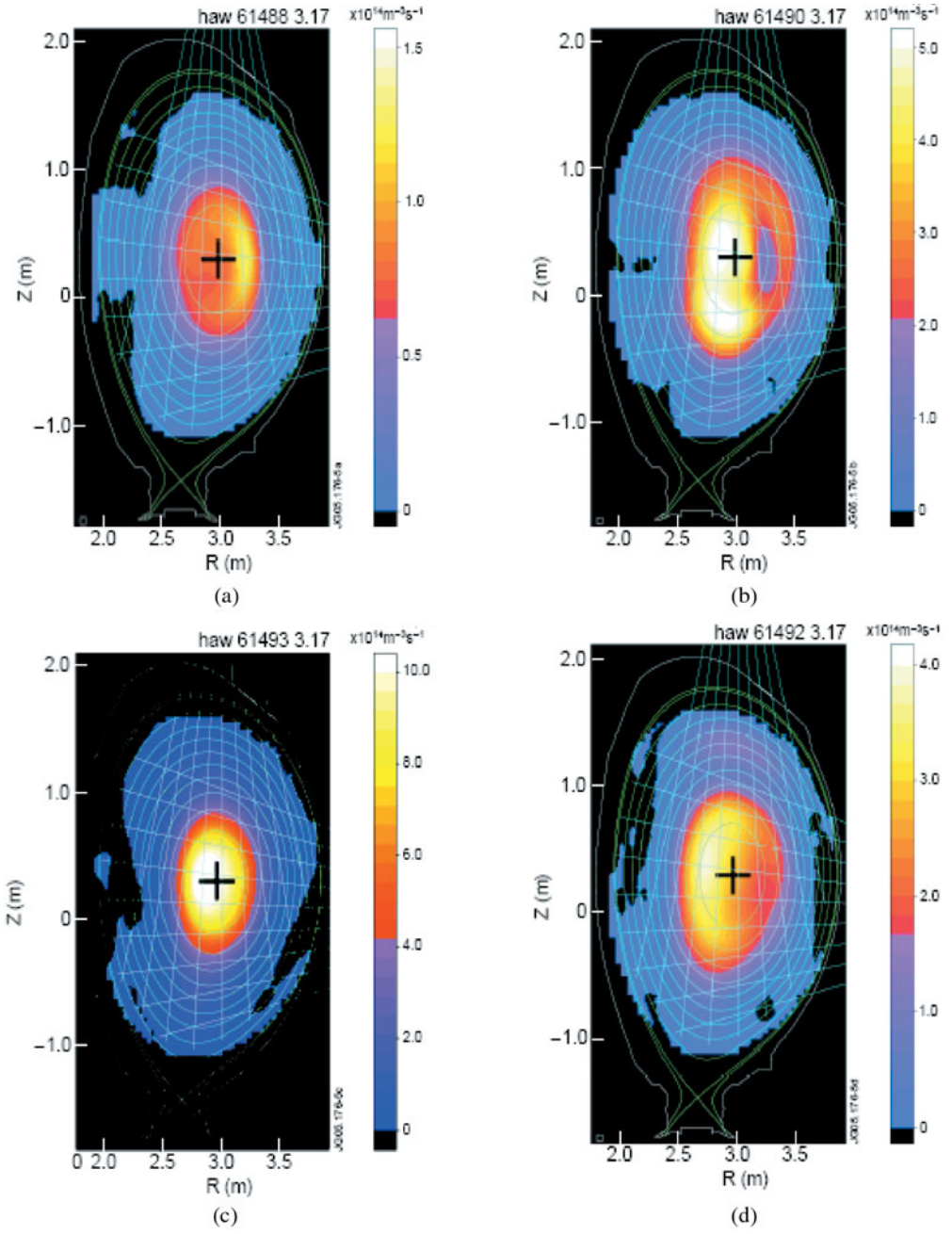

Fig. 15. Tomographic inversions of the Bicron data from the neutron cameras to give 2-D neutron emission profiles: (a) current hole, on-axis injection; (b) current hole, off-axis injection; (c) monotonic current, on-axis injection; and (d) monotonic current, off-axis injection. The + symbol marks the magnetic axis.

magnetic shear.[64] The 2-D neutron source strength and energy distribution measurements in ITER with the required temporal (1 ms for source strength and 0.1 s for energy distribution) and spatial resolutions (10% of the averaged minor radius) can be made by joint application of radial neutron camera[65–67] (RNC) including compact in-plug collimators[68] and vertical neutron cameras[9] (VNC) (Fig. 6).

The RNC consists of 12 × 3 fan-shaped arrays of neutron collimators viewing the plasma through a special shielding plug in equatorial port #1 and additional channels placed inside equatorial port plug[9] #1. All external channels penetrate through the vacuum vessel, cryostat, and biological shield and cross through a single point. Three separate collimator flight tubes (with different diameters in the range of 10 to 40 mm) and detector

housing for each poloidal angle offer a variety of choices of collimator/detector combinations to increase the dynamic range of external RNC measurements. The 12 lines of sight of the RNC are equally spaced (by 30 cm at the plasma center), symmetrically with respect to the plasma equatorial plane. The vertical extension of the plasma coverage by the RNC external channels is 3.3 m from $-0.5 \times b$ to $0.5 \times b$, where b is the minor plasma radius in the vertical direction.

Full plasma coverage in the vertical direction is provided using additional channels placed inside equatorial port plug #1. These channels consist of a stainless steel plus water shielding block containing nine collimators ~140 cm in length and 4 cm in diameter. Four collimators view the plasma above the main external RNC fan of view and another four view from below (see Fig. 6). In this way, the additional channels will provide plasma coverage for $0.5 < \rho < 0.9$ in the upper and lower parts of the plasma, where ρ is the radial coordinate normalized by the averaged plasma radius, a. A ninth collimator viewing the plasma center will be used for cross calibration of the external channels and the additional channels. The detector modules of the additional channels will be placed behind the collimators inside an in-plug shielding block. Because of the strong restriction in maintenance, the most robust and radiation-resistant detectors are under consideration for this application.

Several possible arrangements of the VNC have been studied, including distributed and upper VNC. The main concept of the lower VNC (LVNC) arrangement is to place the VNC shielding module inside a divertor port[9] with collimators viewing the plasma through the gaps in the divertor cassettes, the blanket modules, and the triangular support. The LVNC version shown in Fig. 6 has 10 collimators 35 mm in diameter and ~150 cm in length. The detector block is placed behind the collimators and can be removed for maintenance. All options have essential interfaces with other ITER systems, such as divertor cassette, rail, triangular support, blanket modules, vacuum vessel, and thermal shield. Optimal LVNC arrangement will be decided on the basis of on-going analysis. The results of the MCNP calculations indicated that the discussed LVNC arrangement could provide well-collimated neutron source measurements with application as detectors shown in Table III along with their performance characteristics.

TABLE III

Detectors Considering for Application in ITER Neutron Cameras*

Detector	Housing $\varnothing \times l$ (cm^3)	Sensitivity, cm^2/n	Dynamic Range for 1-ms Time Window	Life Time	Neutron Camera
			For maximum flux 5×10^9 $n/cm^2 \cdot s^{-1}$		
NDD[a] compact spectrometer	$\varnothing 1 \times 2$	2×10^{-5} for single NDD	20 (for 100 ms time window)	10^4 full power seconds	RNC ext RNC int LVNC
NDD flux monitor	$\varnothing 1 \times 2$	10^{-3} for single NDD $2n \times 10^{-3}$ for n NDD + radiator	50 $100 \times n$	2×10^6 full-power seconds $\sim 10^6$ full-power seconds	RNC ext RNC int VNC
CVD[b] diamond detector	$\varnothing 3 \times 3$	2×10^{-2} for detector $\varnothing 25 \times 0.2$ mm^3	1000	2×10^6 full-power seconds	RNC ext RNC int VNC
Stilbene/NE-213 compact spectrometer/monitor	$\varnothing 5 \times 40$	10^{-3} to 1	10 (digital spectrometer for 100 ms) 100 (digital monitor)	?	RNC ext
^{238}U fission chamber	$\varnothing 3 \times 35$	3×10^{-4}	20	Forever	RNC int VNC
ZnS	$\varnothing 5 \times 30$	10^{-3} to 10^{-1}	1	?	RNC ext
Fast plastic scintillator	$\varnothing 5 \times 30$	10^{-3} to 1	100 to 300	?	RNC ext

*See Ref. 9.
[a]NDD = natural diamond detector
[b]CVD = chemical vapor deposition

V. MEASUREMENT OF NEUTRON SPECTRA

V.A. Introduction to Neutron Emission Spectrometry

Important plasma diagnostic information can be obtained from measurements of the energy distribution of the neutron flux from a collimator. Here, the collimator solid angle defines the cone-shaped line volume of the viewed plasma, and the spectrometer at the end of a

collimator records the superposition of spectral characteristic of the local emissivities over the viewed plasma. As the sight line is often directed through the plasma core, which has the highest emissivity, the emission from the plasma core is dominant in the measurements. In addition to this direct plasma emission, the collimated flux includes two types of scattered (indirect) neutron. The viewed part of the opposite side of the plasma vessel is a source of backscattering. Other indirect contributions are due to neutron in-scattering taking place in the collimator walls, plasma port plate, etc.

Then, the neutron emission spectrometry is a multiple-function diagnostic the information of which is derived from measurement of the energy distribution of the direct and scattered flux from the plasma neutron emission,[69,70] F_d and F_s.

The indirect flux data are essential for benchmarking of model calculations of the scattered neutron flux field at locations of interest. This affords important empirical input, for example, for calibration of neutron monitors, i.e., to determine the relationships of their responses to the uncollimated neutron flux received and the total neutron yield rate. The neutron emission spectrometry data are also used for calibrating the flux detectors in the collimator arrays of cameras. The issue here is the admixture of scattered contribution to the measured flux of neutrons of energy above a certain threshold and the benchmarked model calculations are also used to determine the interference (the factor $I_{s/d}$) of the scattered flux in the measured spectrum in the region of overlap with that of direct neutron emission, $F_d(E_n)$. That is, the spectrometer determines $F_n^m(E_n)$ and the value of $I_{s/d}$ such that $F_d(E_n) = F_n^m(E_n) - I_{s/d} \cdot f_s(E_n)$, where $f_s(E_n)$ is the spectral shape from the benchmarked simulations. A good spectrometer should typically allow $I_{s/d}$ to be kept at a level of a few percent in the region of interest to study direct neutron emission, $F_d(E_n)$, measurement of which is the main objective of neutron emission spectrometry diagnostics. The scope and quality of the neutron emission spectrometry information are dependent on spectrometer factors, such as energy resolution and bandwidth, flux detection efficiency, count rate capability, signal-to-background ratio, and calibration. This has set the framework for selection of high-performance spectrometers for use on current fusion experiments and applies also to choosing development objects for ITER.

The spectrum of direct plasma neutron emission reflects the relative motions of the fuel ions given by their velocity distributions. The Maxwellian population of a thermal equilibrium plasma of temperature T_i gives a Gaussian-shaped spectrum of width $W \propto \sqrt{T_i}$ and amplitude (reaction rate) $A \propto n_1 n_2 \langle \sigma v \rangle_{(T_i)}$ where n_1, n_2, are the local ion densities and $\langle \sigma v \rangle$ is the reactivity, as defined in Eqs. (7) and (11), respectively (see Sec. I); this holds for homogenous [constant $Y_n(r)$] plasmas for which profile effects from $Y_n(r)$ are absent. Moreover, the neutron emission from a thermal plasma has a characteristic peak energy, E_c, but plasmas of nonequilibrium ion distributions can produce spectra with tail signatures, such as non-Gaussian shape, energy (Doppler) shift relative to E_c. The latter situation belongs to fuel ion velocity distributions affected by auxiliary heating power (P_{aux}) of NBI or ICRH injection[71] as shown in Eqs. (8) and (10) in Sec. I. These driven plasmas have suprathermal velocity components in the fuel ion populations in addition to the thermal bulk component. In addition, the fuel populations can be in states of rotation apart from having anisotropicity in the pitch angle distribution manifested as Doppler shifts in the neutron spectrum.

Moreover, the population of fast confined alpha particles can give rise to alpha knock-on (AKN) neutron emission in D-T plasmas with a unique signature in the high-energy tail of the spectrum. Fusion product tritons from $d + d \rightarrow p + t$ reactions can form a suprathermal component in the fuel ion population, a fraction of which can suffer nuclear burnup on the bulk deuterons with neutron emission (triton burnup). In a plasma of (pure) deuterium, triton burnup is the sole source of the 14-MeV component of the spectrum, which is a factor of 10^{-3} weaker[6] than the bulk of 2.5-MeV neutrons from $d + d \rightarrow {}^3\mathrm{He} + n$, while it comes in addition to AKN in D-T plasmas. The AKN component in D-T plasma and the triton burnup component in D-T plasma originate from fusion products generated in the plasmas, which we distinguish from fuel ion neutron emission.

The potential D-T plasma parameter information obtainable from neutron emission spectrometry diagnostics is summarized in Table IV (Refs. 69, 70, and references therein). The diagnostic functions are separated into four categories: (A) fuel ion kinetics for plasmas without (A1) and with external heating P_{aux} (A2); (B) confined alpha-particles; (C) the collective motion of the fuel ion population; (D) fusion reactivity parameters; and (E) other support information. The diagnostic functions marked "with a superscript a" in Table IV have been identified as essential for ITER (Ref. 72). The listed functions assume the use of high-performance ideal spectrometers given adequate interface accommodation and viewing access to the plasma; the latter is essentially a requirement on the aperture in the plasma facing wall although the window can be thick, i.e., steel a few millimeters thick is acceptable. The information given in Table IV can be complemented with neutron profile monitors (or neutron cameras), which determine the direct flux as a function of sight line, related to neutron emissivity of the plasma and its radial profile, $Y_n(r)$.

The basic sight line is assumed to be radial with the spectrometer in the equatorial plane or, generally, perpendicular to the magnetic axis, [P]. Some functions require the use of a tangential sight, indicated as [T], or those in which a tangential sight is beneficial as [t] in Table IV. The tangential direction can be either collinear or counter to the anisotropy direction of the ion in neutron emission (e.g., the NBI direction), and so dual

TABLE IV

Summary of Neutron Emission Spectroscopy Diagnostic Functions That Can Potentially Be Performed in D-T Plasmas with Certain Large Spectrometers Complemented with Neutron Camera Data Depending on Interface Access and Sufficiently High Fusion Power

A. *Fuel ion kinetics*
  (A1) Thermal population
    (1) reaction rate
    (2) density product $n_d n_t$ [t]
    (3) Ion temperature[a]
  (A2) Population with significant suprathermal velocity components[b] as A1 plus [t,t2][c]
    (1) suprathermal reaction rate components in addition to reaction rate:A1-(1)
    (2) relative densities of suprathermal velocity components
    (3) suprathermal temperature and ion temperatures (if Maxwellian, otherwise slowing down)

B. *Confined alpha particles [t,t2]*
  (1) amplitude and shape of slowing down distribution[a]
  (2) pressure

C. *Collective motion of fuel ion populations [T,t2]*
  (1) toroidal rotation[a]

D. *Fusion parameters*
  (1) Fusion power[a]; will provide values for *dd* and *dt* reactions separately
  (2) division of fusion power into thermal and suprathermal components [t,t2]
  (3) fuel ion densities in the core (n_d, n_t and n_d/n_t)[d] [t,t2]

E. *Other information*
  (1) the extended spectrum of direct and scattered neutrons from the plasma
  (2) empirical data for benchmarking of flux field calculations.

[a]Diagnostic functions identified as essential for ITER (see Ref. 70).
[b]The framework here is a the phenomenological analysis of the neutron spectrum as due to a bulk component (reactions between thermal ions) and several suprathermal components involving suprathermal velocity components of the fuel population as divided in epithermal and high-energy neutron emission with and without the involvement of anisotropy.
[c]The basic sight line is assumed to be a basic perpendicular sight line [P]; [T] indicates a single tangential sight line is essential and [t] beneficial (beyond gain in statistics) or dual, [T2] and [t2].
[d]Requires simultaneous measurement of 2.5-MeV neutrons from *dd* reactions and 14-MeV from *dt*.

tangential sight lines can be essential [T2]. Taken together, the list given in Table IV assumes the use of up to three spectrometers covering as much as possible of the co/counter angular range in the equatorial plane. The information comes from measurement of the direct and scattered $d + t \rightarrow \alpha + n$ emission over the range $E_n \approx 10$ to 20 MeV except for the function D3 in Table IV, which requires simultaneous measurement of the range $E_n \approx 1.5$ to 5 MeV to cover the 2.5-MeV $d + t \rightarrow {}^3\mathrm{He} + n$ emission.

Extraction of the diagnostic information depends on the complexity of the spectrum where the neutron emission from thermal plasmas is most amenable to analysis (case A1) (Fig. 16a). The interpretation of the results is mostly a matter of handling the profile factor in the line-integrated data, $B(r_{SL})$, which can be obtained quantitatively from cameras. Spectra for plasmas with P_{aux} (Case A2) can be complex, and the ability to analyze them depends on the number of significant components and their relative weights[73] (Figs. 16b and 16c). Thus, the stability of the analysis results depends on the uniqueness of signatures of the underlying ion velocity components. Analysis model dependence can affect the results to varying degrees. However, the neutron spectrometry data can be used the other way around—i.e., the predicted state of the fuel ions and their reactivity are used as input to simulate neutron spectra, which can be confirmed or rejected empirically.

The main issue concerning the AKN component (function B) is the count rate. The AKN, however, was observed during the D-T experimental campaign[74] (DTE1) at JET in plasmas of highest fusion power (5 to 16 MW) at count rate $\leq$10 n/s (Fig. 17). On ITER, we would expect count rates in the range up to 10^4 n/s due to the combination of higher fusion power and electron temperature. The high-energy tails in D-T neutrons would interfere with the AKN spectra depending on the strength and type of P_{aux} applied and the viewing direction as illustrated by the simulations shown in Fig. 18. The triton burnup is not the objective of diagnosis in D-T plasmas

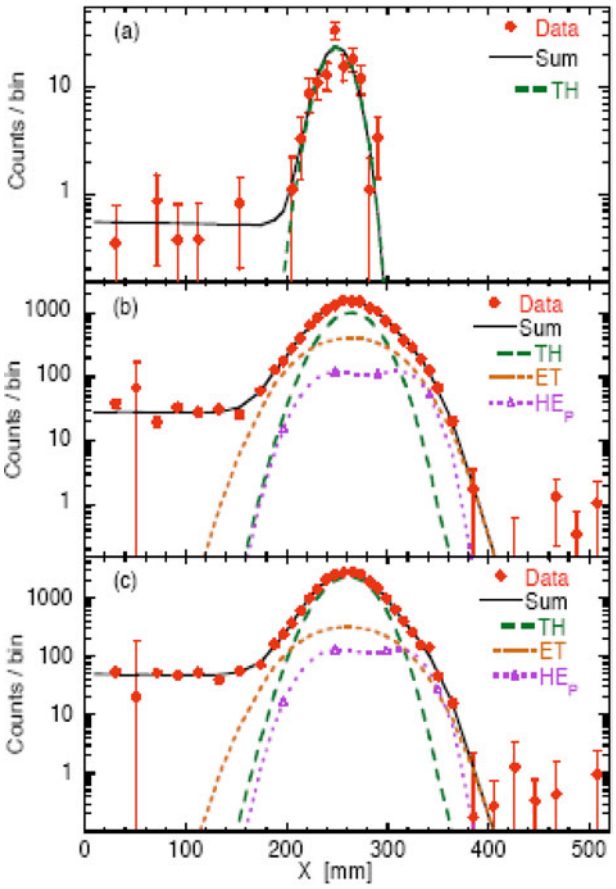

Fig. 16. Measured neutron spectra by MPR for (a) the ohmic, (b) the NBI period, and (c) the D-T plasma generated at JET during the DTE1 campaign. The spectra were analyzed in terms of different neutron emission components generated with assumed velocity components of the fuel ion population. The constant level to the left includes the scattered neutron contribution. The theoretical spectra have been folded with the response function and fitted to the data covering the neutron energy range from 11 to 17 MeV.

but is in D plasmas,[75] where the high-energy tails in D-D neutrons would not interfere.

The main problem with fuel ratio measurement (function D3) is measurement of the 2.5-MeV D-D spectrum, which sits on a scattered neutron continuum (mostly from *dt* D-T reactions) with a peak to continuum ratio[76] of about 1:1. The issues are the low count rate and the ability to subtract from the continuum $F_s(E_n)$ to obtain the remaining D-D component. The continuum is expected to be featureless in the region of interest, the shape of which $f_s(E_n)$ can be obtained from benchmarked neutron model calculations and the amplitude A_s from the measured D-T neutron emission, i.e., $F_d(E_n) = F_n^m(E_n) - A_s \cdot f_s(E_n)$. As we are mostly interested in the ratio of D-D neutron emission to D-T neutron emission, the detailed shape of the D-D spectrum is not essential and the interference from scattered D-D neutrons is insignificant. As A_s can be determined with good statistical accuracy, the limiting concern is the achievable D-D neutron count rate, which is a factor 100 lower than that of *dt* due to the D-D/D-T reactivity ratio. For some detectors, there may be a large difference in detection efficiency between D-D and D-T neutrons [a factor of 6 in the case of the magnetic proton recoil (MPR) discussed below].

Measurement of the fusion power (functions D1&2) by the method discussed here[70] depends crucially on accurate measurement of the energy distribution of a collimated neutron flux $F_n^m(E_n)$ and determination of the direct spectrum $F_d(E_n)$ as described above. The plasma volume contributing to $F_d(E_n)$ is determined by the collimator (sight line and solid angle), in addition to the neutron emission profile, which is obtained from the $B(r_{SL})$ data of cameras. Thus, the relationship between the measured F_n^m (and F_d) and the total neutron rate Y_n can be determined based on ab initio derived factors; as the spectrum is measured for both D-D and D-T neutrons, absolute determination of fusion power in D-T plasmas of any isotopic composition, including pure D, is possible. The main issues are the *absolute* calibration of the spectrometer to determine the collimated flux $F_n^m(E_n)$ and the *relative* calibration of the camera channels to measure the shape of the neutron brightness distribution and the shape of the derived emissivity profile. The method has been tested and applied to neutron spectrometry data from the DTE1 campaign of JET as illustrated by the example shown in Fig. 19. The method is still under development to quantify all systematic error sources with regard to $F_d(E_n)$ and the sensitivity to the plasma profile shapes within the typical range variations as well as extreme cases.

V.B. Spectrometers on Present Tokamaks

Time-of-flight (TOF) is a common neutron spectrometer method and requires the use of two plastic scintillation detectors in fusion applications. The first (S1) is placed in the beam of collimated neutrons flux, of which a fraction is detected through the proton recoil produced in the scattering $n + p_H \rightarrow p_R + n'$, where p_H and p_R denote a proton in the first plastic detector and the recoil proton, respectively. The second detector (S2) is placed at a known distance (L) and records a fraction of the scattered neutrons, again through proton recoil (Fig. 20). A preferred design is to place S1 and S2 on the constant TOF sphere such that the time it takes scattered neutrons to travel from one to the other is $t_2 - t_1 = t_{\mathrm{TOF}}$, where $E_n \propto 1/t_{\mathrm{TOF}}$ is independent of scattering angle α.[a] This is

[a]This comes from the flight path given by $L^2 = 4r^2\cos^2\alpha$ and the scattered neutron energy given by $E_{n'} = 2mr^2\cos^2\alpha/t^2$, which is related to the incident neutron energy through $E_n = E_{n'}/\cos^2\alpha$; relativistic $n + p$ scattering kinematics are assumed and $m_p = m_n = m$. Thus, E_n is $E_n = 2mr^2/t^2$.

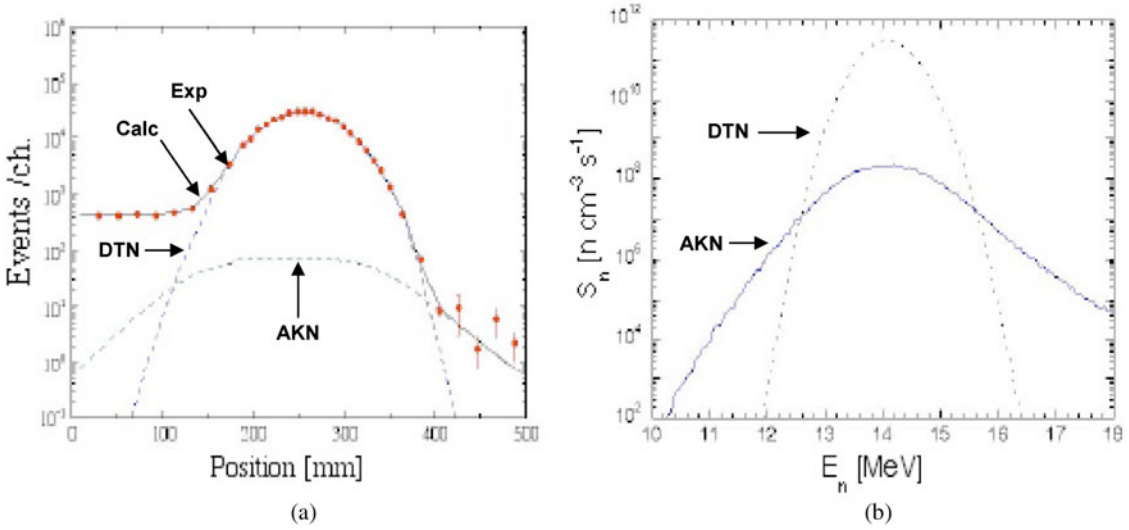

Fig. 17. The measured spectra by MPR for NBH D-T plasmas of the JET DTE1 campaign compared with calculated D-T and AKN components folded with (a) the spectrometer response function and (b) the D-T and AKN components as function of neutron energy.

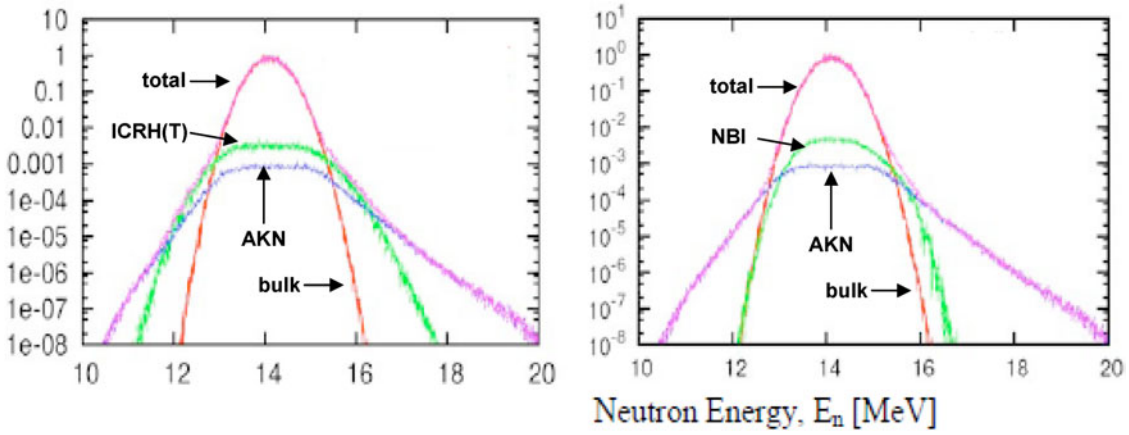

Fig. 18. Predicted spectra of neutron emission from ITER plasmas subjected to ICRH triton heating (upper panel) and NB 1-MeV tritium injection (lower panel). The resulting AKN emission component is shown in comparison with the deuterium-tritium neutrons contributions (thermal bulk and 1% suprathermal). The sight line is assumed to be radial in the midplane (Ref. 70).

the principle behind the TOF spectrometer designed to optimize the count rate (TOFOR) capability[77–79] and in operation at JET since November 2005. It has an estimated count rate capability of a few hundred kilohertz, which will be approached in the flux from maximum power JET D plasmas.

The other possibility is to allow incoming neutrons to scatter from a hydrogen nucleus in S1 and produce charged recoils, such as protons in $n + p_H \rightarrow n' + p$, which carry information on E_n through $E_n = E_p/\sin^2\beta$ where β is the angle between E_n and E_p (with the same assumptions as above and noting that $\beta = 90\text{-}\alpha$) (Refs. 70 and 71). The protons are produced in a thin target, such as foil of polyethylene, placed in the collimated neutron flux; the thickness is set by the minimum proton energy loss $\Delta E_p \ll E_p$ and so E_n can be determined with the desired energy resolution through measurement of E_p of the recoils emitted in a downstream detector at a known angle β. The simplest proton recoil detector for use is a silicon diode placed well outside the beam flux, i.e., $\beta \gg 0$ and so that the angle relative to the foil becomes sufficiently well defined for the required energy resolution. The detector should be sufficiently thick to stop the protons so that E_p can be related to the measured pulse

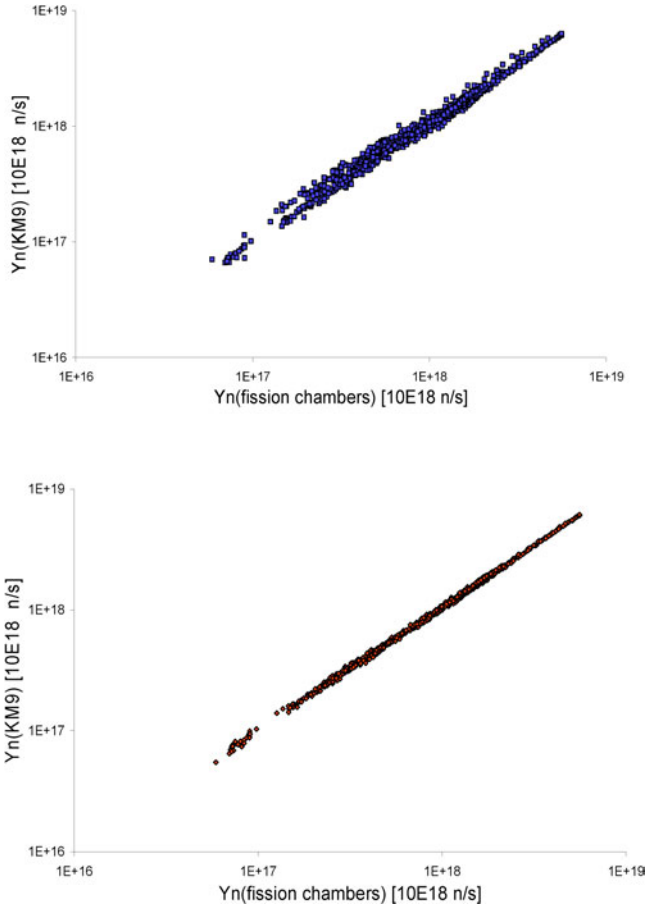

Fig. 19. The neutron yield rate (Y_n) for D-T plasmas of the JET DTE1 campaign obtained by MPR from absolute measurement of the magnitude and the energy distribution of the collimated flux (y-axis) and its correlation with the results from the fission chamber yield monitors. The results were obtained with a neutron emissivity profile of fixed shape and a shape derived from camera data in the lower panel. The maximum yield rate of 6×10^{18} n/s corresponds to a fusion power of 16 MW.

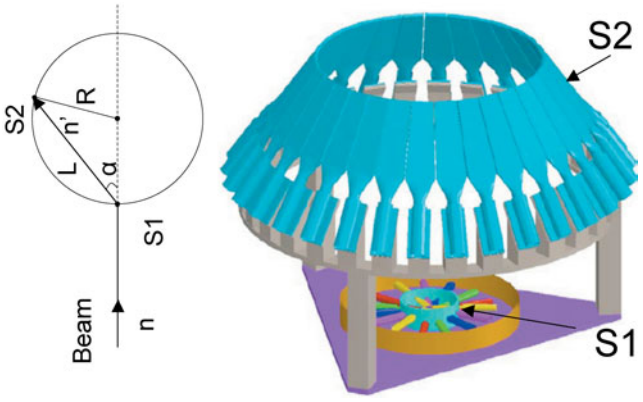

Fig. 20. Principles of the TOF spectrometer showing an incoming neutron being scattered from a proton in scintillator S1 into scintillator S2 at angle α with both detectors placed on the constant TOF sphere (upper panel). The lower panel shows a model of the TOF spectrometer designed for optimized rate (TOFOR); the height is ~1 m (Ref. 70).

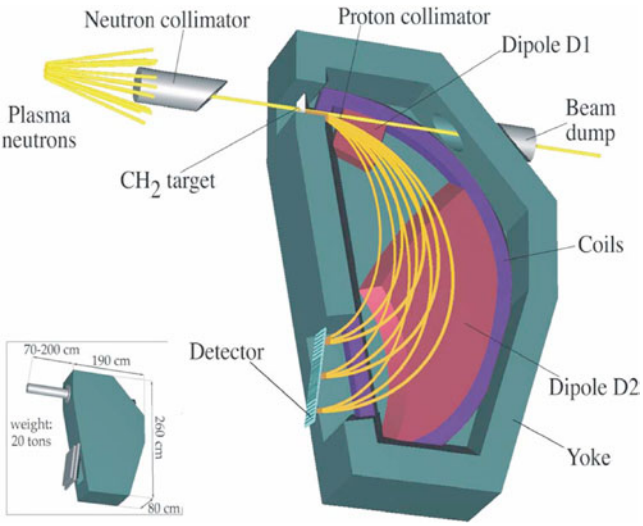

Fig. 21. Model of the MPR spectrometer with the top lid of the yoke removed. The incoming neutrons produce proton recoils in the CH2 target foil. The forward-going protons are focused and monometer analyzed in the pole gap of D1 and D2 magnet and counted in the detector array at the focal plane exit. The upgraded version (MPRu) has a new detector and electronics, which allow measurement of neutrons down to below 2 MeV (Ref. 70).

height. The limiting factors with this recoil technique are the finite spread of β and determination of E_p through pulse height measurement, both of which limit the energy resolution. These limitations are resolved with the MPR method,[80,81] which allows the use of protons emitted at $\beta \approx 0$ deg and the desired situation that $E_n \approx E_p$. The recoil protons are subjected to momentum analysis when they pass from the target to the focal plane of the magnetic spectrometer where they are counted in an array of scintillation detectors (see Fig. 21).

MPR is the most robust method and shows high performance in the aspects mentioned above except for its limited count rate when used with 2.5-MeV $d + d \rightarrow {}^3\text{He}$ neutron emission. A TOF spectrometer is the best choice for neutron spectrometry diagnosis of D plasmas. Different combinations of the TOF and recoil methods have been studied conceptually and have also been applied, but no advantages were observed as fusion neutron

spectrometers over the straightforward TOF method or MPR. The requirement of high performance implies separation of the target for scattering of the neutrons or production of the recoils and the detectors.

It is tempting to use a target that is also the detector so the in situ deposited recoil energy is determined through the measured pulse height. This is the idea underlying the compact spectrometer concept in the form of a thick (several centimeters) hydrogenous scintillation detector[82,83] such as NE213 and stilbene, which have intrinsically distinguishable characteristics with regard to gammas and neutrons. The neutron spectrum can be unfolded from the measured pulse height spectrum.[82,83] However, the situation is complicated because the energy of the recoils does not vary only with E_n but also with the recoil production angle β, which is unspecified. This latter fact distinguishes the compact concept from neutron recoil spectrometers where β is specified giving a one-to-one correspondence between measured E_p and E_n. Recent experimental studies showed that it is possible to compensate for this complication of compact spectrometers by reducing the systematic, statistical, and stability uncertainties in the measurement combined with advancements in the unfolding technique.[83,84] A new method based on digital signal processors showed excellent performance in spectrum measurement with PSD for neutrons and gammas using NE213 detectors.[85,86] A similar system but with a stilbene detector showed high count rate capability in addition to the spectrum measurement and PSD on JT-60 U (Ref. 87).

Since 1983, neutron spectroscopy has been performed at JET (Ref. 82), and at present JET is the tokamak best equipped for neutron spectroscopy diagnostics with two high-performance spectrometers installed. TOFOR (Refs. 77, 78, and 79) is dedicated to measuring 2.5-MeV *dd* neutrons and diagnosis of D plasmas and will reach count rates in the 100-kHz range. It is placed in the roof lab looking vertically down on the plasma at a distance of ~20 m with the sight line perpendicular through the plasma core. There is also an upgrade version[81] of the MPR (MPRu) for measurement of the entire fusion neutron spectrum (≈1.5 to 18 MeV with ±20% coverage in each setting). This is a high-performance instrument for diagnosis of D-T plasmas with count rates up to the megahertz range for full-power discharge; 0.6 MHz was attained in the DTE1 at 16 MW. For D plasmas, it is complementary to TOFOR because of its superior calibration although the count rate will have an expected maximum in the range of a few kilohertz resulting in data of limited statistical accuracy. It has an intermediate sight line at 42 deg to the radial near the equatorial counter to the NBI direction. TOFOR/MPRu combination will allow the first detailed neutron spectroscopy diagnosis plasmas to exploit the anisotropicity in the neutron emission relative to the magnetic field and driven by auxiliary power injection.

V.C. Neutron Spectroscopy Systems on ITER

It is envisaged that neutron spectroscopy will become an essential part of the neutron diagnostic complement for D-T fusion experiments on ITER. Many neutron spectrometer systems[65,88,89] have been considered for ITER. The types chosen will not only affect the scope or quality of the neutron spectroscopy information but also the roles of the other neutron diagnostic systems of yield monitors and cameras. A change in the role of spectrometers is expected in going from JET to ITER as collimated flux measurements would be easier than uncollimated measurements because of access limitations and effective shielding of the plasma radiation. Moreover, the collimated flux measurements with spectrometers and cameras are complementary as exemplified by determination of the (absolute) fusion power through tests at JET; there are likely to be other synergic uses of the neutron diagnostic complement to be developed to give more information than the individual systems alone.

Considering the importance and usefulness of neutron spectroscopy, a relatively large space has been prepared for this purpose outside the main shielding. In addition, a small but sufficient space for compact neutron detectors, capable of energy-resolved measurement, has been prepared at the end of each collimator of RNC and VNC (for details, see Sec. IV; see also Table III). The characteristics of these detectors[88–90] are compared and shown in Table V. The ion temperature profile may be obtained under limited conditions. Information on the behaviors of energetic fuel ions with time and spatial resolution can be obtained by detectors with medium energy resolution[91] or with compact spectrometers such as NE213 or stilbene with dedicated digital signal processors and advanced unfolding processes, as described above. They are especially important to study the abnormality expected in plasma containing ions close to Alfven velocity.

Monitoring of the triton density to deuteron density ratio n_t/n_d in a core plasma is required for burn control in ITER. This can be estimated using D-T and D-D neutron yields, which can be obtained by the separation of D-T and D-D components from a neutron energy spectrum. New neutron detection systems of TOF spectrometers have been developed for measurement of the fuel ratio in burning plasmas, such as ITER (Refs. 92 and 93). In these TOF systems, the key issue is counting rate capability, because the number of D-D neutrons may be only 1/200 to 1/500 that of D-T neutrons. One of the methods to overcome this problem is fast selection of neutrons of interest by pulse-height selection.[92] A test experiment of sophisticated electronics with three discriminators for the first detector was conducted using D-D and D-T neutrons from an accelerator[37] at the FNS at JAEA. Separation of each spectrum in the megahertz region was confirmed experimentally.

TABLE V

Characteristics of Neutron Detection Systems with Energy Resolution*

Neutron Detection Systems	Dimension (typical) (cm)	Energy Resolution	Sensitivity (cm^2/n)	Dynamic Range	Limit by Radiation Damage
Compact Spectrometer					
NDD[88]	$\varnothing 1 \times L2$	2.5%	$\sim 2 \times 10^{-5}$	20 (for 100 ms time window)	5×10^{13} n/cm^2
Scintillation fiber detector[25]	$\varnothing 5 \times L10$	3.3%	$\sim 3 \times 10^{-3}$		5×10^{15} n/cm^2
Medium Spectrometer					
Proton recoil[81,82]	$\varnothing 40 \times 40$	2.2%	10^{-4}	5×10^{9}	10^{15} n/cm^2
COTETRA[90]	$\varnothing 10 \times 40$	6%	10^{-3}		10^{15} n/cm^2
Proton recoil with microchannel	$\varnothing 20 \times 40$	2%	10^{-5}	5×10^{10}	5×10^{15} n/cm^2
Large Spectrometer					
MPR[70]	$200 \times 200 \times 300$	2%	$\sim 5 \times 10^{-5}$	5×10^{10}	5×10^{15} n/cm^2
TOF (TOFHR)[70]	$200 \times 200 \times 100$	1.6%			
TOF for DD/DT[91,92]	$50 \times 50 \times 100$	20%	10^{-4}		

*They are divided into three categories by size. Large spectrometers are supposed to be located outside the main shield, but medium and compact systems can be set at the end of each collimator of the neutron camera.

Some of the neutron spectroscopy capabilities of large-sized high-performance spectrometers MPR, which have been demonstrated at JET, could be used with similar sight lines and collimator solid angles. However, a recent inventory gave negative results regarding an alterative high-performance spectrometer for the 14-MeV technique[70] because of difficulties in obtaining sufficient flux in the MPR collimator for a given neutron yield rate with the diagnostic-machine interface imposing sight line limitations and the spatial resolution limiting the plasma volume to be viewed.

In broad terms, the current plasmas of most interest for neutron spectroscopy measurements are those strongly driven by auxiliary power injection. On ITER, the objective is to reach plasmas that require little auxiliary power beside alpha heating, which should be ideally suited for neutron spectroscopy studies as well as experiments to reach this stage and fusion optimization of the plasma.

VI. MEASUREMENT OF GAMMA RAYS

VI.A. Introduction to Gamma-Ray Measurement

One of the most important techniques used for studying fast ion behaviors in fusion devices is nuclear reaction gamma-ray diagnostics.[94] Measurements on the tokamaks Doublet-III (Ref. 95), TFTR (Refs. 96 and 97), JET (Refs. 98 and 99), and JT-60U (Ref. 100) have shown that an intense gamma-ray emission is produced when fast ions (fusion products, ICRF-driven ions, and NBI ions) react either with plasma fuel ions or with plasma impurities, such as beryllium, boron, carbon, and oxygen. On JET, the gamma-ray emission measurements were first reported by Sadler et al.[98] and have since been used to interpret different fast ion physics effects arising during ICRF and NBI heating.[101]

There are three sources of fast particles that can give rise to gamma-ray emissions from plasmas. First, fusion reactions [see Eqs. (1) through through(4)] between the plasma fuel ions produce fusion products, such as fast tritons, protons, ^{3}He, and ^{4}He ions with energies in the mega-electron-volt range. Second, ICRF heating of H and ^{3}He minority ions accelerates these ions to energies in the mega-electron-volt range. There are also ICRF schemes to accelerate D, T, and ^{4}He ions. Third, NBI heating introduces D, T, H, ^{4}He, and/or ^{3}He ions. Fast ions born in plasmas produce line spectra due to their nuclear reactions with low-Z plasma impurities. The fusion product neutrons interact with the structural materials, generating a continuous gamma-ray background. Typical gamma-ray spectra recorded during ICRF heating with ^{3}He ions are shown in Fig. 22. The 17-MeV gamma rays from the D(^{3}He, γ) ^{5}Li reaction, used in JET as an indicator of the ICRF power deposition efficiency, were observed.

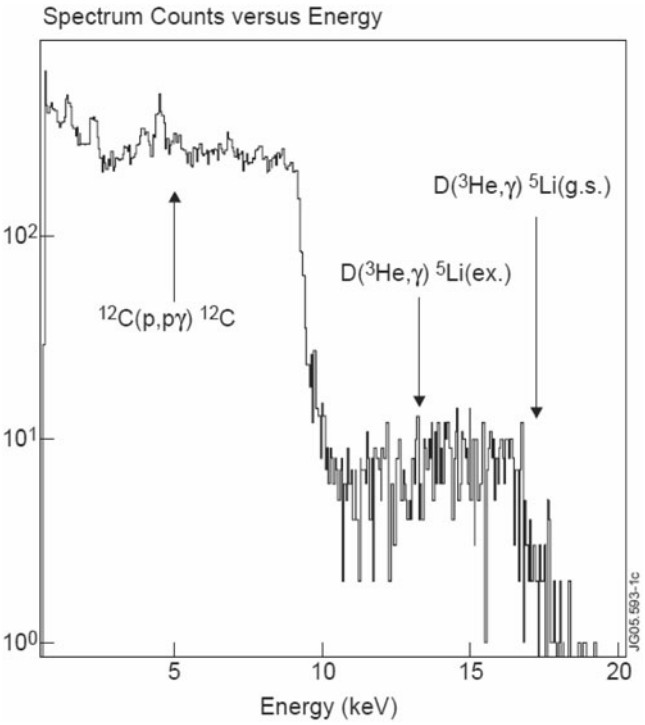

Fig. 22. Sum of four gamma-ray energy spectra measured during discharges with ICRF heating tuned to $\omega = \omega_{c^3\mathrm{He}}$ in deuterium JET plasma with high ^{3}He concentration $\eta_{\mathrm{He}} = 20\%$ (Ref. 104).

A list of all essential nuclear reactions, which have been identified in the gamma-ray spectra recorded at JET, is given in Table VI. These reactions are classified by the types of fast ions interacting with different target ions in plasma. The nuclear reaction energies, the Q values (Q^*), which characterize the mass balance of the reactions, are also presented there and can be used for assessment of the excitation energy of the residual nuclei. In general, the energy in the center-of-mass frame for a reaction $a(b,c\gamma)d$ is given by $E = Q^* + E_a + E_b - E_c - E_d$, where $Q^* = (M_a + M_b - M_c - M_d)c^2$ and M_i $(i = a,b,c,d)$ is the rest mass of the nucleus involved in the reaction. Table VI also contains assessments of the minimum energy of the fast particles required to produce gamma-ray yields, at levels that can be measured in JET.

Particularly, Table VI shows the reaction ^{9}Be$(\alpha,n\gamma)$ ^{12}C, the significance of which was investigated in detail for the fusion-born alpha-particle measurements.[102] This reaction is a resonant reaction, which has thresholds. The presence of the 4.44-MeV peak in the gamma-ray spectra is evidence for the existence of alphas with energies exceeding 1.7 MeV. The 3.21-MeV gamma rays indicate that alphas with energies in excess of 4 MeV exist in the plasma. As an example, Fig. 23

TABLE VI

Nuclear Reactions Identified in Gamma-Ray Spectra Recorded at JET

Reaction	Energy of Reaction, Q, and Intensive Gammas (MeV)	E_{min} (MeV)[a]
Protons		
$D(p,\gamma)^3He$	5.5 γ5.5	0.05
$T(p,\gamma)^4He$	19.81 γ20	0.05
$^9Be(p,p'\gamma)^9Be$	−2.43 γ1.7, γ2.4	3
$^9Be(p,\gamma)^{10}B$	6.59 γ6.8, γ7.5	0.3
$^9Be(p,\alpha\gamma)^6Li$	2.125 γ3.6	2.5
$^{12}C(p,p'\gamma)^{12}C$	−4.44, −7.65 γ4.4, γ3.2	5.8
Deuterons		
$^9Be(d,p\gamma)^{10}Be$	4.59 γ3.4	0.5
$^9Be(d,n\gamma)^{10}B$	4.36 γ2.9, γ3.6	0.5
$^{12}C(d,p\gamma)^{13}C$	2.72 γ3.1, γ3.7, γ3.9	0.9
Tritons		
$D(t,\gamma)^5He$[b]	16.63 γ17	0.02
$^9Be(t,n\gamma)^{11}B$	9.56 γ7.3	0.5
^3He Ions		
$D(^3He,\gamma)^5Li$	16.38 γ17	0.1
$^9Be(^3He,n\gamma)^{11}C$	7.56 γ4.8	0.9
$^9Be(^3He,p\gamma)^{11}B$	10.32 γ7.3	0.9
$^9Be(^3He,d\gamma)^{10}B$	1.09 γ2.9, γ3.6	0.9
$^{12}C(^3He,p\gamma)^{14}N$	4.78 γ2.3, γ5.1	1.3
Alphas		
$^9Be(^4He,n\gamma)^{12}C$	5.70 γ4.4, γ3.2	1.7,4.0

[a]Assessment of the minimal fast particle energy needed for a gamma-ray observation at JET.

[b]This reaction is a branch of the main fusion reaction $D(T,n)^4He$ with the neutron to gamma ray ratio is about 10^5:1. Thus, 17-MeV gamma rays in the same way as neutrons carry the information about fusion performance and alpha particle birth profile.

shows two gamma-ray spectra, recorded in the same JET discharge: the left plot shows the spectrum during 300-ms T-beam blip, while the right plot shows the spectrum just after the NBI blip. During the injection two gamma-ray peaks 4.44 and 3.21 MeV were observed because the alpha energy exceeded 4 MeV due to the conservation of momentum even though the energy of the T-beam was in the ~100-keV region. In the post-blip time slice, however, the 3.21-MeV peak became rather weak. This is an effect of changes in the distribution function, i.e., the result of a shift of the high-energy tail to the low-energy range due to alpha-particle slow-down.

VI.B. Gamma-Ray Measurement on Present Tokamaks

The fusion gamma-ray spectra recorded at Doublet-III (Ref. 95) employed a detector consisting of an NaI(Tl) crystal 5 cm in diameter and 5 cm in length viewed with a PMT. The detector was placed in a lead collimator 4 m from the machine center viewing the plasma tangentially. During hydrogen NBI heating, 5.5-MeV gammas from the reaction $D(p,\gamma)^3He$ were observed.

In TFTR, NaI(Tl) and NE226 detectors were used for gamma-ray measurements.[96,97] The detectors were enclosed in a compact blockhouse on the test cell floor with overall dimensions of approximately 2 m (width) × 2 m (length) × 1 m (height) and consisting of nested strata of concrete, polyethylene, lithium carbonate, and lead. The detectors viewed the TFTR vacuum vessel through a cylindrical collimator 1.5 m in length and 20 cm in diameter in the blockhouse. The NaI(Tl) crystal scintillator 10 cm in diameter and 10 cm in height was used for background gamma-ray measurements. The fusion gammas during deuterium NBI heating of ^3He plasmas were observed with a cylindrical cell of liquid fluorocarbon scintillator NE226 measuring 12.7 cm in length × 12.7 cm in diameter. This is a neutron-insensitive scintillator with rapid decay constant (about 2 ns), and the peak energy resolution and detection efficiency for gamma rays up to 19 MeV have been reported.[94]

In JT-60U, H-ions were accelerated by second harmonic ICRF heating up to several mega-electron-volts. Gamma-ray spectra in the energy range of 1 to 20 MeV were measured using a NaI(Tl) scintillator measuring 12.7 cm × 12.7 cm (5 in. × 5 in.) surrounded by a 50-cm polyethylene and 30-cm lead shield.[100,103] In the JET tokamak gamma-ray energy spectra are measured with two different devices, one with a horizontal and one with a vertical line of sight through the plasma center.[104] The first spectrometer is a calibrated BGO scintillation detector with diameter of 75 mm and a height of 75 mm that is located in a well-shielded bunker and views the plasma tangentially. To reduce the neutron flux and the gamma-ray background, the front collimator is filled with polyethylene. Behind the scintillation detector, there is an additional dump of polyethylene and lead. The gamma rays are recorded continuously in all JET discharges over the energy range from 1 to 28 MeV, with an energy resolution of ~4% at 10 MeV. The second device for gamma-ray energy spectrum measurements is a NaI(Tl) scintillation detector with a diameter of 125 mm and a height of 150 mm, which views the plasma vertically through the center.

The spatial distribution of the gamma-ray emission sources in the JET plasma is measured using the neutron profile monitor (see Fig. 13), which is routinely used for neutron and gamma-ray measurements. The monitor consists of two cameras, vertical and horizontal, with nine and ten lines of sight, respectively. The radiation detectors are NE213 liquid scintillators.

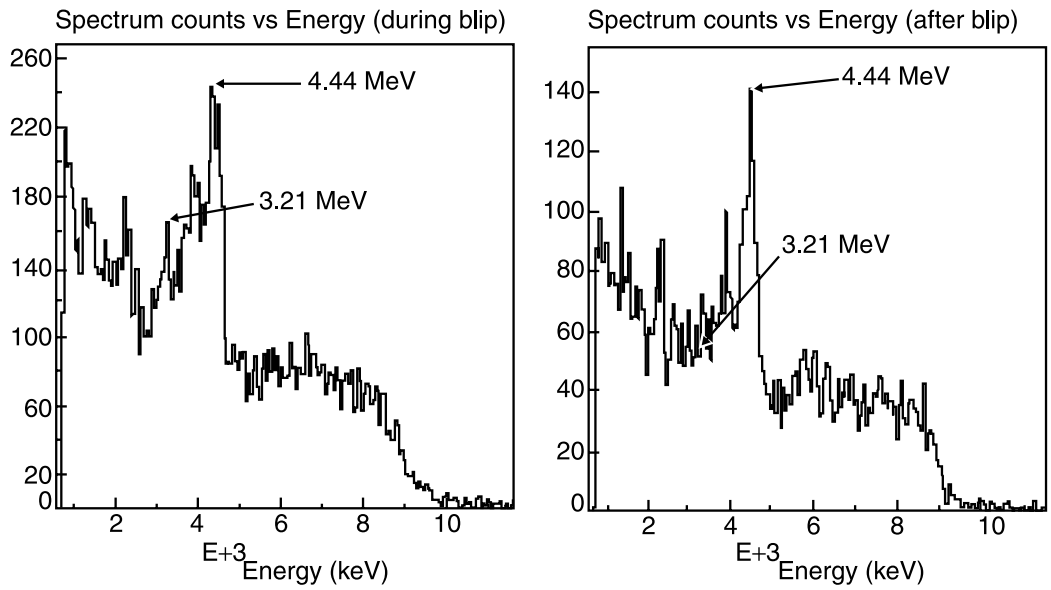

Fig. 23. Gamma-ray spectra measured in JET discharge with deuterium NBI heating and tritium 300-ms blip (Ref. 103).

Although the JET profile monitor was developed for neutron measurements and the shielding and detectors are not entirely adequate for gamma-ray measurements, in some discharges with ICRF only heating gamma-ray measurements are possible by exploiting the different pulse-shape characteristics exhibited by NE213 for neutrons and gamma-rays. The standard PSD electronic modules were set up to restrict the detection of the gamma-ray emission to the energy range 1.8 to 6 MeV. It was shown that the discrimination between neutrons and gamma rays, which are produced by ICRF-accelerated fast ions, is acceptable for further analysis if their count rates are comparable. Now at JET, to measure the gamma-ray emission profile in the energy range $E\gamma >$ 1 MeV, we use the fast electron bremsstrahlung diagnostic system, which is incorporated into the neutron profile monitor. The detector array is comprised of 19 CsI(Tl) photodiodes (10 mm $\times$ 10 mm $\times$ 15 mm). The photodiodes are placed remotely for measurements in the front of neutron detectors within each collimation channel. The data acquisition system accommodates the gamma-ray count-rate measurement in four energy windows. This allows allocating specific gamma-ray peaks in the windows to be counted separately. A typical example of the tomographic reconstruction of the measured line-integrated profiles is shown in Fig. 24. It can be seen clearly that the gamma-ray emission profile[105] produced by fast D ions (right figure) differs from the profile from ^{4}He ions (left figure) accelerated by ICRF. This effect can be explained by the difference in pitch angle distribution between ^{4}He beam-ions injected quasi tangentially into the plasma and isotropic D-minority ions.

VI.C. Measurement Systems on ITER

The gamma-ray diagnostics based on $D(t,\gamma)^5He$ and $^9Be(\alpha,n\gamma)^{12}C$ reactions could provide important information on behavior of the fusion alpha particles in ITER, as proposed in Refs. 100 and 101, where Be impurity is supplied from the FW. The main idea of the technique consists of a comparison of both the 3.5-MeV alpha-particle birth profile (17-MeV gamma rays) and that of the confined alpha particles slowed down to 1.7 MeV (4.4-MeV gamma rays). These measurements could be performed with a dedicated gamma-ray profile camera, which is similar to the neutron/gamma camera currently in operation at JET. For time-resolved profile measurements, efficient gamma-ray spectrometers and neutron attenuators, in each channel of the cameras, are needed. General requirements of the spectrometers are high efficiency and peak-to-background ratio. It could be a single crystal spectrometer with heavy scintillator or a detector-array[106] like GAMMACELL based on the highly radiation-resistant BaF_2 scintillators, which allow measurement of gamma rays in the energy range from 1 to 30 MeV. The feasibility of the measurements also depends on the quality of neutron suppression of the collimators. Water is a simple neutron filter with no carbon content, but 14-MeV neutrons will activate this attenuator, and the 6.13-MeV gamma-ray background will become problematic. A more convenient neutron filter is based on ^{6}LiH. It is

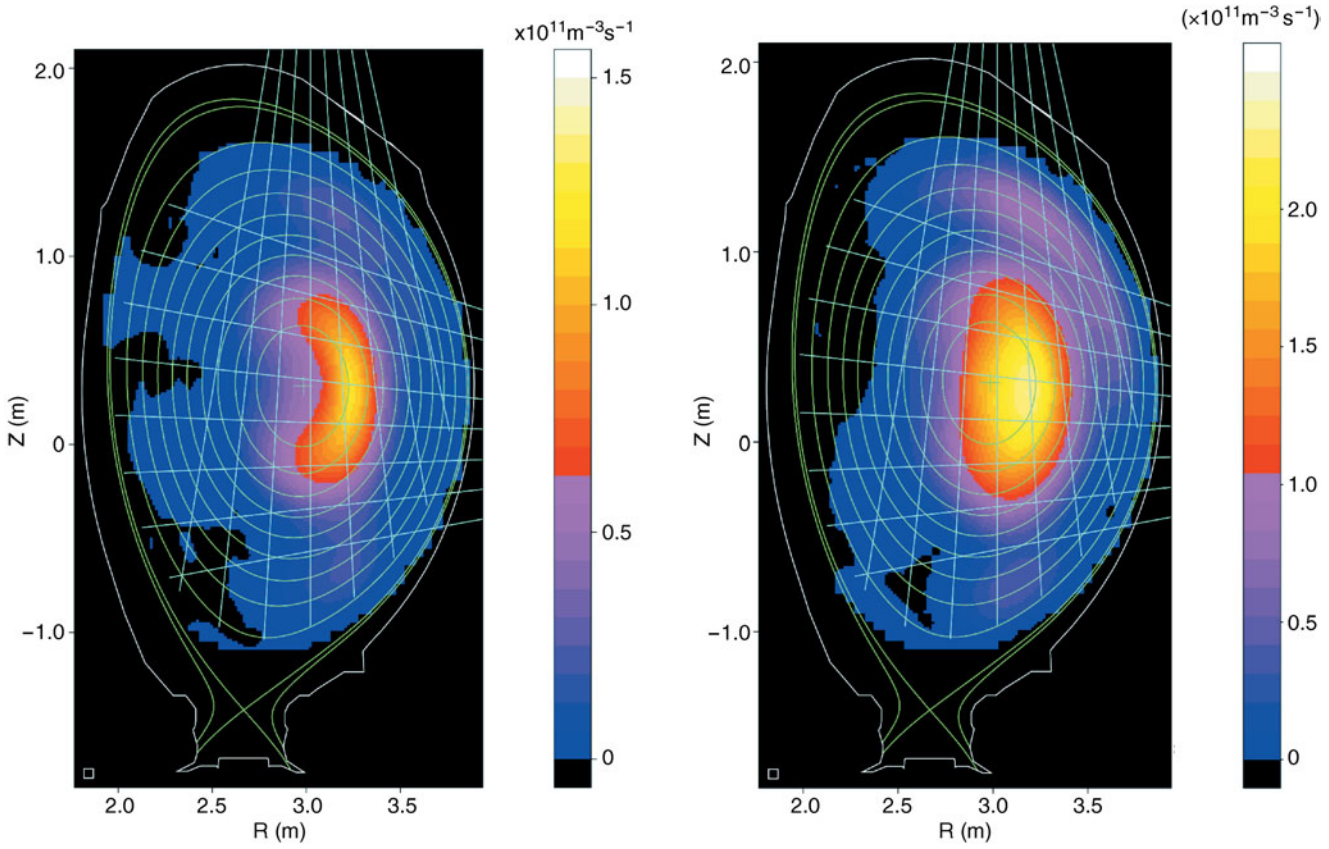

Fig. 24. Tomographic reconstructions of 4.44-MeV gamma-ray emission from the reaction $^{9}\mathrm{Be}(^{4}\mathrm{He}, n\gamma)^{12}\mathrm{C}$ (left) and 3.09-MeV gamma-ray emission from the reaction $^{12}\mathrm{C}(\mathrm{D}, p\gamma)^{13}\mathrm{C}$ (right) deduced from simultaneously measured profiles (Ref. 105).

compact, effective, and transparent for gamma rays and does not produce interfering gamma rays in the high-energy range. A 30-cm sample of the ^{6}LiH filter reduces 2.4-MeV neutron flux to ~900 times and the 15-MeV neutron flux to ~30 times.[101,107]

Gamma-ray measurements at the JT-60U tokamak during experiments with deuterium NBI heated plasmas[100] showed that use of these plugs reduced the neutron-induced gamma-ray background by a factor of 10. Gamma-ray cameras with such neutron filters seem to be the best candidates for measuring gamma-ray spectra in the presence of high neutron fluxes typical of D-T reactor plasmas.

The gamma cameras could be integrated with radiation shields of radial and vertical neutron cameras and have the same type of fan-shaped viewing geometry. Each gamma-ray detector module should have a separate line of sight with two adjustable collimators and intermediate flight tube, allowing gamma-ray spectrometry over a wide operating range. The collimators need to be individually rotatable to set the appropriate collimation and neutron/gamma suppression depending on the task.

Gamma-ray spectroscopy induced by alpha particles from a boron sample placed on the FW using $^{10}\mathrm{B}(\alpha, p\gamma)^{13}\mathrm{C}$ reaction was proposed by Kiptily et al. to measure the lost alpha strength.[108] Study of realistic detection system, specially the shielding and transportation of signals is awaited.

VII. MEASUREMENT OF LOST ALPHAS

VII.A. Introduction to Alpha Particle Loss

Fast ions, such as heating ions and alpha particles, should be well confined until they transfer their energy to the plasma. In particular, alpha heating will be needed to sustain ignition in fusion reactor plasma. Fundamental confinement properties can be studied by measurement of the alpha-particle loss[7,109] From the viewpoint of machine protection, it is important to monitor the bombardment location and the heat load on the FW (Ref. 8). A clear understanding of loss mechanism is required to carry the fusion program to a real reactor. The temporal behavior of lost alpha signals, and measurement of pitch angle and energy distribution will be useful to understand the underlying physics,[7] such as first orbit loss,[109,110] toroidal field ripple loss,[111] ICRH-induced loss,[112] and MHD-induced loss.[113,114]

VII.B. Examples of Fast Ion Loss Measurement Systems

VII.B.1. Fusion Reactivity Measurement

Since the early 1980s, measurement of protons produced by $d(d,p)t$ and $d(^3\mathrm{He},p)$ fusion was used to diagnose plasmas in the PLT (Refs. 115 and 116), DIII-D (Ref. 110), JIPPTII-U (Ref. 117), and ASDEX (Ref. 118) using silicon surface barrier detectors installed in metal cases on vacuum vessels. In these experiments, fusion-produced fast ions were not confined, but the fusion reaction rate and their spatial information were obtained by measurement of these fusion-produced fast ions, and useful information on the heating efficiency and heating schemes could be obtained. By using the intrinsic energy resolution of these detectors, the ion temperature or slowing-down processes of heating ions were studied by measuring the lost ion spectra.

VII.B.2. Confinement Study and MHD Loss Measurement

In large tokamaks, such as TFTR or JET, a substantial portion of the fusion-produced fast ions were confined. Similar but more dedicated probes were developed,[109] and classical confinement properties, MHD-induced losses, ripple effects, etc., were studied. For example, scintillation probes[109,112] were developed for TFTR, and alpha-particle loss measured by a detector located at the TFTR vessel bottom showed dependence of loss ratios on the plasma current in the ion grad-*B* drift direction.[114] As these probes were capable of resolving the energy and pitch angles of escaping fast ions with good time resolution, there has been a great deal of study of the MHD-induced losses. The pitch angle and energy-resolved lost ion measurement results were compared with calculations using full-gyromotion orbit codes and characterized. Most of these studies are reviewed in Ref. 7.

The experience of TFTR was transferred to other tokamaks, such as JFT-2M (Ref. 119), ASDEX (Ref. 120), and NSTX (Ref. 121), and helical devices, such as CHS (Refs. 122 and 123) and LHD (Ref. 124). Figure 25 shows a schematic diagram of the scintillator-type lost fast ion probe of the compact helical system (CHS). Light emitted from the scintillator is divided by a beam splitter into two detection paths and is detected by the PMT array and charge-coupled device (CCD) camera. The PMT signals have high time resolution up to 20 kHz. The 2-D image obtained with the CCD camera provides information on both gyroradius and pitch angle simultaneously. Ions with larger gyroradii hit the scintillator surface farther from the aperture than those with smaller gyroradii. Ion impact points are dispersed across the line passing through the center of two apertures according to the pitch angles of detected ions. The experimental results clearly showed that the maximum ion energy corresponded to that of the injected beam and that the ion losses were induced by MHD, as shown in Fig. 26. Moreover, their pitch angle distribution showed that two types of ions, passing boundary ions and trapped ions, were lost periodically during an $m/n = 3/2$ fishbone-like instability.

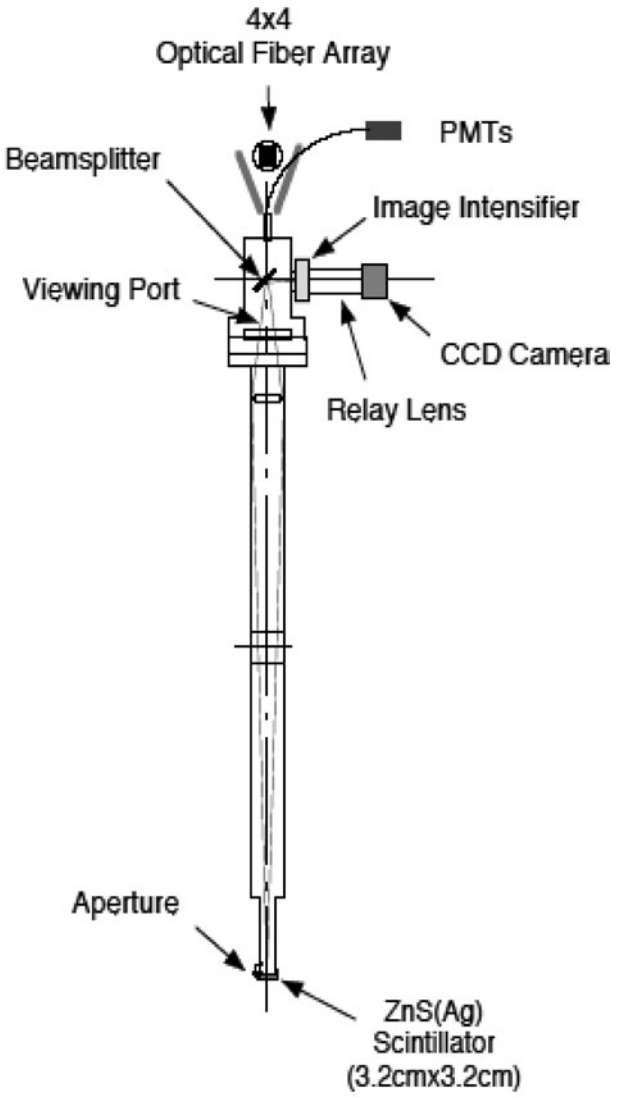

Fig. 25. Schematic diagram of the scintillator-type lost fast ion probe of CHS. Light emitted from the scintillator is divided by a beam splitter into two detection paths and is detected by the PMT array and CCD camera (Ref. 123).

A new type of lost ion probe based on multichannel thin foil Faraday collectors has recently been developed, and has been used to investigate ion losses on NSTX (Ref. 125), DIII-D (Ref. 126), and JET (Ref. 127). These detectors, in which ions that are lost from a fusion plasma are detected as current, are intended to study lost ions in general and *d-t* fusion product alpha particles. Figure 27

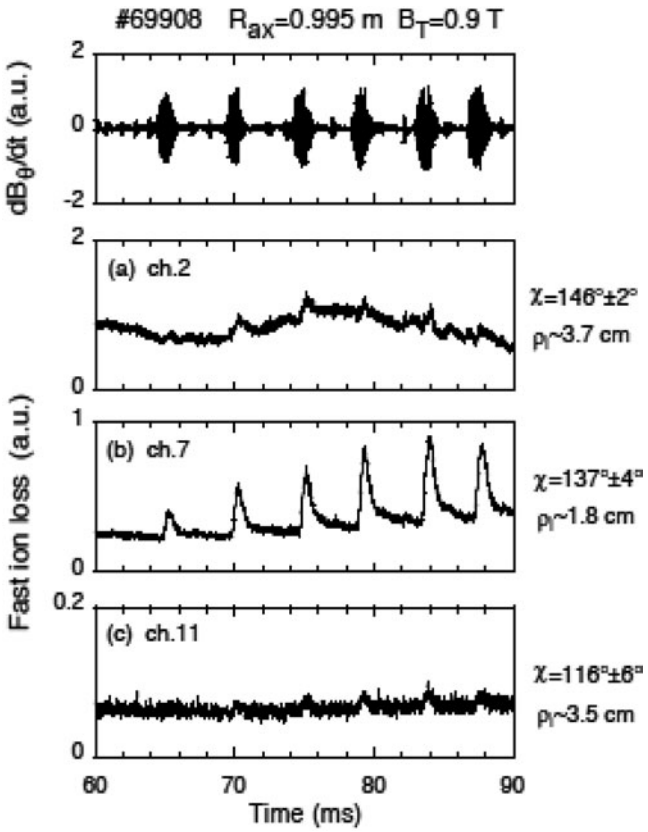

Fig. 26. Time traces of the magnetic fluctuation and fast ion losses for specific pitch angles and energies measured with the scintillator probe on CHS during energetic particle mode activity. The largest spikes are seen on signals from the boundary of passing orbits (Ref. 123).

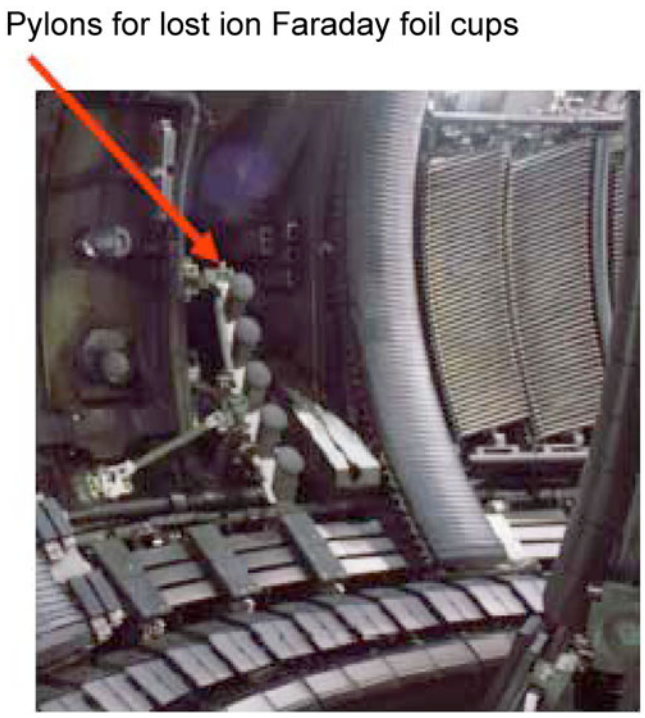

Fig. 27. Lost ion Faraday cup detectors (Ref. 128).

shows a photograph of the array of JET Faraday foil lost ion probes.[128]

VII.C. Lost Alpha Measurement Systems of ITER

The self-heating of a D-T plasma by fusion-produced alpha particles is the key to the realization of self-sustainable ignition of a thermonuclear plasma for fusion reactors. The loss of alpha particles means deterioration of the heating input power. Moreover, the localization of alpha-particle bombardment on the FW surface may induce serious damage. This is one of the key problems in ITER. However, the severe thermal/radiation environment of measurement location and the difficulties with regard to access and installation limit the application of conventional measurement tools.[8]

Strong localization of alpha-particle bombardment on the FW surface of ITER has been predicted.[8] The loss location is ~200 deg in poloidal angle with toroidally enhanced bombardment between adjacent toroidal field coils. Here, the poloidal angle is defined with the inner midplane being 0 deg. It is important not only to monitor the bombardment location (loss imaging) for machine protection but also to measure the pitch angle, energy distribution, and temporal behavior during MHD to understand the underlying physics.

Some diagnostic candidates for lost alpha-particle measurement, such as camera imaging of scintillators on the FW, scintillator probes, Faraday cups, and imaging bolometers,[8,129,130] have been studied for integration on ITER. Camera imaging of scintillators fixed on the FW will provide a bombardment image enhanced by alpha particles.[129] Figure 28 shows the geometry of the scintillator imaging system on a computer-aided design (CAD) drawing of ITER. Ceramic scintillators are fixed in holes on the edges of the FW (Cu backing) of blanket modules #16 and #17 and viewed by a mirror system connected to a filtered camera. Ceramic scintillators, which are covered by a thin ceramic layer protection against low-energy ions/neutral particles, may be used to enhance alpha-particle signals above the background. The alpha-particle gyromotion guiding into a hole and the scintillator surface in the hole directed toward the camera will also help to discriminate alpha signals. It is necessary to carry out the full gyro-orbit calculation in time reverse including the actual shape of the modules to determine whether orbits starting from the detection point return to the plasma. An infrared camera can be used to monitor loss, but there is no discrimination of alpha signals from other ions.

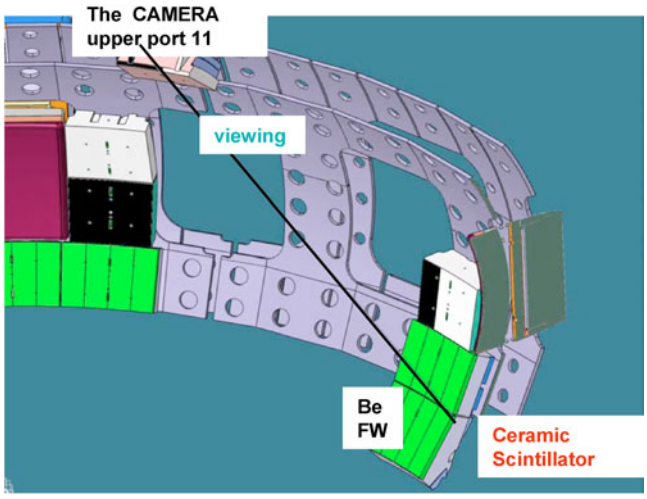

Fig. 28. CAD drawing showing integration of the scintillator imaging system. The upper port 11 is used for the viewing camera, and the ceramic scintillators are fixed behind the edge of the FW of blanket modules #16, and #17 (Ref. 129).

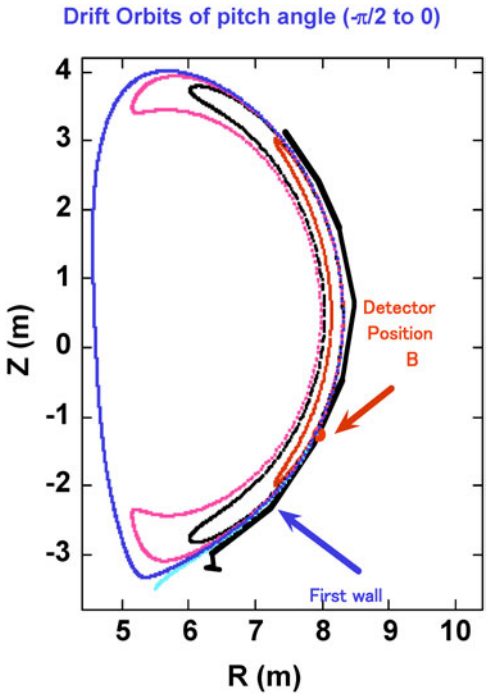

Fig. 29. Drift orbits of escaping alpha particles calculated from the detector position on the slits in the front panels of the blanket module #16 with in time inverse (Ref. 129).

A new type of ceramic scintillator has been developed. The characteristics of ceramic sheets in which scintillation materials are blended have been tested using a plasma source and a low-energy helium beam of 3 MeV up to 400°C. However, scintillation efficiencies are degraded by continuous bombardment of ion beams. The scintillation spectrum, the efficiency to electrons, and the efficiency to ions are dependent on the materials blended. Technology for sintering of scintillators into transparent ceramics is currently under development, and it has been shown that preheating of scintillator material mitigates the degradation of luminescence.[131]

Candidate measurement tools for time-resolved pitch angle and energy measurement of lost alphas include Faraday cups and scintillator probes. Orbits starting time inversely from the blanket gap between #16 and #17, as shown in Fig. 29, return to the plasma, and suitable positions for these probes are close to the blanket gap. Working models are currently in preparation for examination at JET, as mentioned above. Neutron-induced noise on the Faraday cup probe has been examined theoretically and is ~2% against maximum loss. It is considered that dummy probes are necessary because radiation-induced current and radiation-induced electric motive force may pose problems for current measurement in the nA range. Twisted cables should be tested. In addition, a cooling system should be designed for the scintillators because they will be exposed to temperatures above 300°C.

VII.D. Confined Alpha-Particle Measurement on ITER

Measurement of confined alpha particles is also essential to examine the heating source and to predict the self-sustainable burning plasma for fusion reactors. As alpha particles are confined in the plasma, an active method should be used to obtain spatial information, and this has attracted a great deal of attention from the viewpoints of transport studies, internal transport barrier studies, and alpha-particle–driven and/or pressure-driven instabilities. Velocity distribution is also important for analyses of Alfven instabilities.

However, this is a serious challenge in ITER. Several measurement methods have been proposed and their feasibilities have been studied[8] as shown in Table VII, but as yet none of these methods have proven satisfactory. One of the most active methods is collective Thomson scattering (CTS). Several approaches have been proposed. Kondoh et al. proposed use of a high-power CO_2 laser (50 J, 10 Hz) with a scattering angle of 0.5 deg injected from the divertor port.[132] Other groups have proposed use of 50 to 65 GHz beams in the X-mode from a tunable gyrotron[133,134] or launching 1 to 2 MW at 180 GHz (Ref. 135). In CTS measurement, the velocity distribution of ions is obtained.

There have been several proposals based on charge exchange recombination spectroscopy. This method is based on measuring the line emission from single-charge exchange reactions between beam particles and alpha particles, and measurement on TFTR showed that this is a useful tool to obtain slowed-down alpha particles.[136,137] A method that uses the 1-MeV ITER heating beam[138]

TABLE VII
Comparison of Various Methods to Measure Confined Alpha Particles

	Source	S/N at $\rho = 0$ for Best Shot	Energy Range	Abs. n_α	Δr	Δv	Δt	Comments
Requirement					<0.1 yr	10%	<100 ms	
Collective Thomson scattering	50 to 60 GHz gyrotron	1 to 10	1 to 3 MeV		Yes	Yes	Yes	O-mode
	CO_2 high power laser 50 J, 10 Hz		1 to 3 MeV		0.3 yr	Yes	2 ms	Forward angle detection
	1 to 2 MW at 180 GHz							ECE background
Charge exchange recombination	Heating beam		0.8 to 2 MeV			Yes	Yes	$v_{//}$, only
	DNB		Thermal		Outer region	Yes	Yes	Outer region
Double charge exchange beam neutralization	1.7 MeV $^3He^0$ from 10 mA $^3He^-$	10 (3 MeV)	1 to 3 MeV	Yes	0.1 yr	2.5%	<100 ms	Beam development machine integration $v_{//}$ only
AKO By MPR		?	1 to 3 MeV	?		No	?	Contamination of beam ions** Low efficiency
AKO by neutral analyzer					No	Above threshold		
AKO by bubble detector					No	Above threshold	No	
Gamma (4.4 MeV)	Be		>1.7 MeV		Yes	Above threshold	<100 ms	Background estimation Be density

could be applied for measurement of high-energy (0.8 to 2.4 MeV) alpha particles moving in the direction close to the heating beam because the charge exchange cross section decreases rapidly as the energy of relative motion of beam deuterons and alpha particles increases above 200 keV. The same method can be used to measure the velocity distribution of thermalized alpha particles using the lower energy (100 keV) diagnostic neutral beam[139] (DNB). Double charge exchange neutralization with high-energy neutral beams has also been proposed.[140] This method uses a tangential ^{3}He beam with energy of 0.8 to 1.5MeV injected from ITER equatorial port 6 (Ref. 141). This method can be realized only when this port is available. In addition, activity on intense beam development is required.

The AKN measurements are an indirect method using elastic scattering between alpha particles and fuel ions producing energetic deuterons or tritons. The suprathermal ions react to form neutrons with energies above the 14-MeV birth energy forming a high-energy knock-on tail in the neutron energy distribution. This method was described in detail in Sec. V. There are proposals to measure knock-on energetic ions neutralized by the 1-MeV heating beams or by electron capture from intrinsic impurities to obtain integrated information on alpha-particle confinement.[142] Another technique measures the energetic knock-on neutron tail due to alphas using the lengths of the proton recoil tracks produced by neutron collisions in nuclear emulsions.[142] Alpha-particle measurement by gamma-ray spectroscopy is described in Sec. VI.

VIII. SUMMARY

Fusion product measurements, measurements of neutrons, gamma rays, and escaping mega-electron-volts ions produced in D-D, D-T, and other nuclear reactions are commonly used for diagnosing fusion plasmas magnetically confined. In D-D experiments on present devices, fusion reaction between a thermal and a nonthermal ion and that between nonthermal ions contribute substantially to the fusion reaction rate. Many interesting studies on energetic ion behaviors have been done by fusion product diagnostics. For D-T fusion experiments on ITER, where the neutron emission rate will increase by more than an order of 10^3 from present large tokamaks and the thermonuclear fraction will be boosted as the self-heating source from alpha particles becomes dominant, the fusion product diagnostics will be more important and will play the essential role, not only on the measurement of the fusion output power, but also on self-heating burning plasma studies. The combination of neutron emission rate measurement, profile neutron emission measurement, activation measurement, and careful calibration experiments will provide the absolute fusion output and fusion fluence on the FW from a fusion device. Because

the neutron flux at detectors will be larger by an order of 2 to 6 than that of typical experiments on large present devices, the time, spatial, or energy resolution will be improved, and various dedicated measurements become possible. High time-response measurements can be used for burn control and MHD studies. Neutron emission spectroscopy measurement have potential to provide other information such as ion temperatures, fusion-produced alpha-particle behaviors, fuel ion densities, and so on.

Measurement of confined alpha particles is essential to examine the heating source into the plasma and to predict the self-sustainable burning plasma for fusion reactors. Several measurement methods have been proposed for ITER and their feasibilities have been studied, but as yet none of these methods have proven satisfactory. Lost alpha measurement is challenging on ITER but important to understand the underlying physics of the loss and to avoid the localization of alpha-particle bombardment, which may induce serious damage on the FW.

ACKNOWLEDGMENTS

This work was supported by a grant-in-aid from the Ministry of Education, Culture, Sports, Science, and Technology of Japan Priority Area of Advanced Burning Plasma Diagnostics Program, and EURATOM-UKAEA Fusion Association, Abingdon, United Kingdom, and under the auspices of the European Fusion Development Agreement with financial support from the Swedish EURATOM Association, the Swedish Research Council, and Uppsala University, Uppsala, Sweden.

REFERENCES

1. L. I SCHIFF, *Quantum Mechanics*, Chap. II, McGraw-Hill, New York.

2. L. M. HIVELY, *Nucl. Fusion*, **17**, 873 (1977).

3. A. KRAUSS et al., *Nucl. Phys.*, **A 465**, 150 (1987).

4. H-B. BOSCH and G. M. JALE, *Nucl. Fusion*, 611 (1992).

5. G. GAMOV, *Z. Phys.*, **51**, 204 (1928).

6. O. N. JARVIS, *Plasma Phys. Control. Fusion*, **36**, 209 (1994).

7. W. W. HEIDBRINK and G. J. SADLER, *Nucl. Fusion*, **34**, 535 (1994).

8. M. SASAO et al., *Plasma Phys. Control. Fusion*, **46**, S107 (2004).

9. A. V. KRASILNIKOV et al., *Nucl. Fusion*, **45**, 1503 (2005).

10. T. NISHITANI et al., *Rev. Sci. Instrum.*, **63**, 5270 (1992).

11. G. F. KNOLL, *Radiation Detectors*, John Wiley and Sons, New York (1979).

12. Y. ENDO, T. ITO, and E. SEKI, *IEEE Trans. Nucl. Sci.*, **NS-29**, 714 (1982).

13. "A General Monte Carlo N-Particle Transport Code," LA-12625-M, J. B. BRIESMEISTER, Ed. Los Alamos National Laboratory (1997)

14. O. N. JARVIS, G. SADLER, P. VAN BELL, and T. ELEVANT, *Rev. Sci. Instrum.*, **61**, 3172 (1990).

15. H. W. HENDEL et al., *Rev. Sci. Instrum.*, **61**, 1900 (1990).

16. J. D. STRACHAN et al., *Rev. Sci. Instrum.*, **61**, 3501 (1990).

17. D. L. JASSBY et al., *Rev. Sci. Instrum.*, **66**, 891 (1995).

18. R. J. GOLDSTON et al., *J. Comput. Phys.*, **43**, 61 (1981).

19. Report JAERI-M, **91-159**, 104, Naka Fusion Research Establishment, Japan Atomic Energy Research Institute (1991).

20. T. NISHITANI *Nucl. Fusion*, **34**, 1069 (1994).

21. W. W. HEIDBRINK et al., *Nucl. Fusion*, **28**, 1897 (1988).

22. S. CONROY, O. N. JARVIS, G. SADLER, and G. B. HUXTABLE, *Nucl. Fusion*, **28**, 2127(1988).

23. C. W. BARNES et al., *Nucl. Fusion*, **38**, 597 (1998).

24. T. NISHITANI et al., *Proc. 14th Int. Conf. Plasma Phys. and Controlled Nuclear Fusion Research*, Wüzburg, 1992, Vol. 1, p. 351 (1993).

25. T. NISHITANI et al., *Plasma Phys. Control. Fusion*, **38**, 355 (1996).

26. T. NISHITANI, K. EBISAWA, T. IGUCHI, and T. MATOBA, *Fusion Eng. Des.*, **34–35**, 567 (1997).

27. M. YAMAUCHI, T. NISHITANI, K. OCHIAI, Y. MORIMOTO, J. HORI, K. EBISAWA, and S. KASAI, *Rev. Sci. Instrum.*, **74**, 1730 (2003).

28. K. ASAI, T. IGUCHI, K. WATANABE, J. KAWARABAYASHI, T. NISHITANI, and C. I. WALKER, *Rev. Sci. Instrum.*, **75**, 3537 (2004).

29. K. ASAI, T. IGUCHI, J. KAWARABAYASHI, K. WATANABE, T. NISHITANI, and C. WALKER, *Fusion Eng. Des.*, **81**, 1497(2006).

30. B. ESPOSITO et al., *Rev. Sci. Instrum.*, **70**, 1130 (1999).

31. M. J. LOUGHLIN et al., *Rev. Sci. Instrum.*, **70**, 1126 (1999).

32. M. PILLON, M. MARTONE, O. N. JARVIS, and J. KÄLNE, *Fusion Technol.*, **15**, 1420 (1989).

33. C. W. BARNES, A. R. LARSON, and A. L. ROQUEMORE, *Fusion Technol.*, **30**, 63 (1996).

34. M. HOEK, T. NISHITANI, Y. IKEDA, and A. MORIOKA, *Rev. Sci. Instrum.*, **63**, 885 (1995).

35. C. W. BARNES, M. J. LOUGHLIN, and T. NISHITANI, *Rev. Sci. Instrum.*, **68**, 577 (1997).

36. T. NISHITANI, K. EBISAWA, and S. KASAI, *Rev. Sci. Instrum.*, **74**, 1734 (2003).

37. J. KANEKO et al., *Rev. Sci. Instrum.*, **72**, 809 (2001).

38. Y. VERZILOV et al., presented at Neutron Working Group Meeting, 10 ITPA, Moscow, Russia, April 11, 2006.

39. S. VON GOELER et al., *Rev. Sci. Instrum.*, **68**, 548 (1997).

40. M. J. LOUGHLIN et al., *Rev. Sci. Instrum.*, **70**, 1124 (1999).

41. F. D. BROOKS, *Nucl. Instrum. Methods*, **162**, 477 (1979).

42. J. M. ADAMS and G. WHITE, *Nucl. Instrum. Methods*, **156**, 459 (1978).

43. A. L. ROQUEMORE et al., *Rev. Sci. Instrum.*, **61**, 3163 (1990).

44. L. C. JOHNSON, *Rev. Sci. Instrum.*, **63**, 4517 (1992).

45. A. L. ROQUEMORE et al., *Rev. Sci. Instrum.*, **66**, 916 (1992).

46. S. VON GOELER et al., *Rev. Sci. Instrum.*, **67**, 473 (1996).

47. A. L. ROQUEMORE et al., *Rev. Sci. Instrum.*, **68**, 544 (1997).

48. M. ISHIKAWA et al., *Rev. Sci. Instrum.*, **73**, 4237 (2002).

49. YU. A. KASCHUCK, B. ESPOSITO, L. A. TRYKOV, and V. P. SEMENOV, *Nucl. Instrum. Methods*, **476**, 511 (2002).

50. J. M. ADAMS et al., *Nucl. Instrum. Methods*, **329**, 277 (1993).

51. O. N. JARVIS, J. M. ADAMS, F. B. MARCUS, and G. J. SADLER, *Fusion Eng. Des.*, **34–35**, 59 (1997).

52. J. M. ADAMS et al., *Nucl. Instrum. Methods*, **A329**, 277 (1993).

53. S. POPOVICHEV et al., *Proc. 31st EPS Conf. Plasma Physics*, London, United Kingdom, 28G, P5-173 (2004).

54. K. D. ZASTROW et al., *Plasma Phys. Control. Fusion*, **46**, B255 (2004).

55. G. BONHEURE et al., *Nucl. Fusion*, **46**, 725 (2006).

56. P. U. LAMALLE et al., *Proc. 31st EPS Conf. Plasma Physics*, London, United Kingdom, 28G, P5-165 (2004).

57. R. S. GRANETZ and P. SMEULDERS, *Nucl. Fusion*, **28**, 457 (1988).

58. F. B. MARCUS et al., *Plasma Phys. Control. Fusion*, **33**, 277 (1991).

59. L. C. INGESSON et al., *Nucl. Fusion*, **38**, 1675 (1998).

60. N. C. HAWKES et al., *Plasma Phys. Control. Fusion*, **47**, 1475 (2005).

61. J. MLYNAR et al., *Plasma Phys. Control. Fusion*, **45**, 169 (2003).

62. J. MLYNAR et al., *Fusion Eng. Des.*, **74**, 781 (2005).

63. G. BONHEURE, et al., *Nucl. Fusion*, **46**, *7*, 725 (July 2006).

64. A. V. KRASILNIKOV, in *Diagnostics for Experimental Thermonuclear Fusion Reactor 2*, p. 439, P. E. STOTT et al., Eds., Plenum Press, New York (1998).

65. L. C. JOHNSON et al., in *Diagnostics for Experimental Thermonuclear Fusion Reactor 2*, p. 409, P. E. STOTT et al., Eds., Plenum Press, New York (1998).

66. F. B. MARCUS et al., in *Diagnostics for Experimental Thermonuclear Fusion Reactor 2*, p. 419, P. E. STOTT et al., Eds., Plenum Press, New York (1998).

67. L. PETRIZZI et al., Contract FU06 CT 2003-00020, EFDA/02-1002 (Aug. 2004).

68. A. V. KRASILNIKOV et al., *Instruments and Experimental Techniques*, **47**, *2* (2004).

69. J. KÄLLNE, "Study of Neutron Spectrometers for ITER," UU-INF #10/05, Uppsala University, Uppsala, Sweden (Nov. 2005).

70. L. GIACOMELLI et al., *Nucl. Fusion*, **45**, 1191 (2005).

71. T. ELEVANT and J. SCHEFFEL, *Diagnostics for Experimental Thermonuclear Fusion Reactor 2*, p. 429, P. E. STOTT et al., Eds., Plenum Press, New York (1998).

72. "Design Description Document of Diagnostics," N55DDD201-07-05W0.3. 5.5.8, Neutron Diagnostics, DDD 5.5B ITER (2001).

73. H. HENRIKSSON et al., *Plasma Phys. Control. Fusion*, **47**, 1 (2005).

74. J. KÄLLNE et al., *Phys. Rev. Lett.*, **85**, 1246 (2000).

75. L. BALLABIO et al., *Nucl. Fusion*, **40**, 21 (2000).

76. J. KÄLLNE et al., *Rev. Sci. Instrum.*, **62**, 2871 (1991).

77. G. GORINI and J. KÄLLNE, *Rev. Sci. Instrum.*, **63**, 4548 (1992).

78. A. HJALMARSSON et al., *Rev. Sci. Instrum.*, **74**, 1750 (2003).

79. M. GATU et al., *Rev. Sci. Instrum.*, **77**, 10E702 (2006).

80. G. ERICSSON et al., in *Advanced Diagnostics for Magnetic and Inertial Fusion*, p. 121, P. E. STOTT et al., Eds., Kluwer Academic/Plenum Publishers, New York (2002).

81. H. SJÖSTRAND et al., *Rev. Sci. Instrum.*, **77**, 10E717 (2006).

82. O. N. JARVIS, *Nucl. Instrum. Methods A*, **476**, 474 (2002).

83. H. KLEIN et al., "Scintillation Detectors for Fast Neutrons," PoS(FNDA2006) 097; available on the Internet at http://pos.sissa.it/

84. L. BERTALOT et al., *32nd European Conf. Controlled Fusion and Plasma Physics*, Tarragona, Spain, Vol. 29C, p-1.078.

85. B. ESPOSITTO et al., *Rev. Sci. Instrum.*, **75**, 3350 (2004).

86. B. ESPOSITTO et al., *Nucl. Instrum. Methods*, **518**, 626 (2004).

87. T. ITOGA, "Development of Fast Counting System for Neutron Emission Profile," PhD Thesis, Tohoku University (2007).

88. T. ELEVANT et al., *Diagnostics for Experimental Thermonuclear Fusion Reactors I*, p. 445, P. E. STOTT et al., Eds., Plenum Press, New York (1995).

89. A. V. KRASILNIKOV et al., *Diagnostics for Experimental Thermonuclear Fusion Reactors I*, p. 435, P. E. STOTT et al., Eds., Plenum Press, New York (1995).

90. N. NAOI et al., *Rev. Sci. Instrum.*, **77**, 10E704 (2006).

91. M. OSAKABE et al., *Rev. Sci. Instrum.*, **66** , 920 (1995).

92. K. OKADA et al., *Rev. Sci. Instrum.*, **77**, 10E726 (2006).

93. K. ASAI et al., *Rev. Sci. Instrum.*, **77**, 10E721 (2006).

94. S. S. MEDLEY and H. HENDEL, *Bull. Am. Phys. Soc.*, **26**, 980 (1982).

95. D. E. NEWMAN and F. E. CECIL, *Nucl. Instrum. Methods*, **227**, 339 (1984).

96. F. E. CECIL and S. S. MEDLEY, *Nucl. Instrum. Methods*, **271**, 628 (1988).

97. S. S. MEDLEY et al., *Rev. Sci. Instrum.*, **61**, 3226 (1990) .

98. G. J. SADLER et al., *Fusion Technol.*, **18**, 556 (1990).

99. O. N. JARVIS et al., *Nucl. Fusion*, **36**, 1513 (1996).

100. T. KONDOH et al., *J. Nucl. Mater.*, **241–243**, 564 (1997).

101. V. G. KIPTILY, F. E. CECIL, and S. S. MEDLEY, *Plasma Phys. Control. Fusion*, **48**, R59 (2006).

102. V. G. KIPTILY et al., *Phys. Rev. Lett.*, **93**, 115001 (2004).

103. T. KONDOH et al., *1998 ICPP & 25th European Conference on Controlled Fusion and Plasma Physics (Praha). ECA*, Vol. 22C, 1478 (1998).

104. V. G. KIPTILY et al., *Nucl. Fusion*, **42**, 999 (2002).

105. V. G. KIPTILY et al., *Nucl. Fusion*, **45**, L21 (2005).

106. V. G. KIPTILY et al., *Plasma Dev. Oper*, **7**, 255 (1999).

107. V. G. KIPTILY et al.,*Tech. Phys.*, **43**, 471 (1998).

108. V. G. KIPTILY et al., *Diagnostics for Experimental Thermonuclear Fusion Reactors 2*, p. 511, P. E. STOTT et al., Eds., Plenum Press, New York (1997).

109. S. J. ZWEBEN, *Nucl. Fusion*, **29**, 825 (1989).

110. H. H. DUONG and W. W. HEIDBRINK, *Nucl. Fusion*, **33**, *2*, 211 (Feb. 1993).

111. K. TOBITA et al., *Nucl. Fusion*, **34**, 1097 (1994).

112. D. S. DARROW et al., *Nucl. Fusion*, **36**, 1 (1996).

113. H. H. DUONG et al., *Nucl. Fusion*, **33**, *5*, 749 (May 1993).

114. S. J. ZWEBEN et al., *Plasma Phys. Control. Fusion*, **39**, A275 (1997).

115. R. E. CHRIEN et al., *Phys. Rev. Lett.*, **46**, 535 (1981).

116. W. W. HEIDBRINK et al., *Nucl. Fusion*, **27**, 129 (1987).

117. M. SASAO, "Plasma Diagnostics," Sec. 9.2, Japan Society of Plasma Science and Nuclear Fusion Research, Ed., (1990) (in Japanese).

118. H. BOSCH, *Rev. Sci. Instrum.*, **61**, 1699 (1990).

119. K. SHINOHARA et al., *Plasma Phys. Control. Fusion*, **46**, S31 (2004).

120. M. GARCÍA-MUÑOZ et al., *Nucl. Fusion*, **47**, L10 (2007).

121. D. S. DARROW et al., *Rev. Sci. Instrum.*, **72**, 784 (2001).

122. M. ISOBE et al., *Rev. Sci. Instrum.*, **70**, 827 (1999).

123. T. KONDOH et al., *Nucl. Fusion*, **40**, 1575 (2000).

124. M. NISHIURA et al., in *9th IAEA-Technical Mtg. Energetic Particles in Magnetic Confinement Systems*, Takayama, Japan, November 9–11, 2005; available on the Internet at http://dg1.nifs.ac.jp/IAEATM-EP2005/program.html, P-23 (2005).

125. W. W. HEIDBRINK et al., *Nucl. Fusion*, **43**, 883 (2003).

126. W. P. WEST et al., *J. Nucl. Mater.*, **337–339**, 420 (2005).

127. O. N. JARVIS et al., *Fusion Technol.*, **39**, 84 (2001).

128. D. S. DARROW et al., *Rev. Sci. Instrum.*, **77**, 10E701 (2006).

129. M. SASAO et al., in *9th IAEA-Technical Mtg. on Energetic Particles in Magnetic Confinement Systems*, Takayama, Japan, November 9–11, 2005; available on the Internet at http://dg1.nifs.ac.jp/IAEATM-EP2005/program.html, OT11 (2005).

130. B. J. PETERSON et al., in *9th IAEA-Technical Mtg. on Energetic Particles in Magnetic Confinement Systems*, Takayama, Japan, November 9–11, 2005; available on the Internet at http://dg1.nifs.ac.jp/IAEATM-EP2005/program.html, P-24 (2005).

131. M. NISHIURA et al., *Rev. Sci. Instrum.*, **77**, 10E720 (2006).

132. T. KONDOH et al., *Rev. Sci. Instrum.*, **74**, 1642 (2003).

133. F. MEO et al., *Rev. Sci. Instrum.*, **75**, 3585 (2004).

134. S. B. KORSHOLM et al., *Rev. Sci. Instrum.*, **77**, 10E514 (2006).

135. U. TARTARI, in *Diagnostics for Experimental Thermonuclear Fusion Reactors I*, p. 513, P. E. STOTT et al., Eds., Plenum Press, New York (1995).

136. G. M. McKEE et al., *Phys. Rev. Lett.*, **75**, 649 (1995).

137. G. M. McKEE et al., *Nucl. Fusion*, **37**, 501 (1997).

138. S. TUGARINOV et al., "Analysis of Alpha Particles and Fast Beam Deuterons Distribution Measurements by Using CXRS on ITER Heating Beams," *30th EPS Conf. Controlled Fusion and Plasma Physics*, Saint Petersburg, Russia, July 7–11, 2003, European Physical Society (2003).

139. M. VON HELLERMANN et al., *Rev. Sci. Instrum.*, **77**, 10E516 (2006).

140. M. SASAO et al., *Nucl. Fusion*, **35**, 1629-24 (1996).

141. M. SASAO et al., *Rev. Sci. Instrum.*, **77**, 10E130 (2006).

142. R. K. FISHER, *Rev. Sci. Instrum.*, **75**, 3556 (2004).